Applied Catalysis B: Environmental 185 (2016) 322–336

Contents lists available at ScienceDirect

Applied Catalysis B: Environmental

journal homepage: www.elsevier.com/locate/apcatb

Synergetic effect of Pd addition on catalytic behavior of monolithic platinum–manganese–alumina catalysts for diesel vehicle emission control

S.A. Yashnik[a,*], S.P. Denisov[b], N.M. Danchenko[b], Z.R. Ismagilov[a]

[a] Boreskov Institute of Catalysis, Pr. Lavrentieva, 5, Novosibirsk 630090, Russia
[b] Plant of Automotive Catalysts, Dzerzhinskogo st., 2, Novoural'sk 624130, Russia

ARTICLE INFO

Article history:
Received 31 August 2015
Received in revised form
26 November 2015
Accepted 10 December 2015
Available online 14 December 2015

Keywords:
Manganese–alumina catalyst
Pt and Pd catalysts
Synergetic effect
Diesel emission control
Catalytic converter
Multicomponent catalyst
Washcoated catalyst

ABSTRACT

The advanced diesel emission control catalyst Pt–Pd–MnO_x–Al_2O_3 has been developed on the basis of the synergetic effect of Pt with Pd and manganese oxides observed in hydrocarbon and carbon monoxide oxidation reactions. This effect allows a decrease in the total loadings of Pt and Pd down to 0.52 g/L in the monolithic catalyst, providing high activity in low temperature oxidation of light hydrocarbons and high thermal stability.

The catalytic activity of Pt–Pd–MnO_x–Al_2O_3 monolithic catalysts in butane oxidation and DIESEL tests depends on the Pt and Pd precursors, their individual loadings and their ratio (Pt/Pd). For a selected Pt precursor at its content 0.17 g/L, the catalytic performance of Pt–Pd–MnO_x–Al_2O_3 catalyst improves with an increase in Pd loading from 0 to 0.35 g/L and is nearly constant at a higher Pd loading (0.70 g/L). The most active monolithic Pt–Pd–MnO_x–Al_2O_3 catalyst is prepared by using platinum-dinitrodiamine and palladium nitrate solutions as noble metal precursors.

The catalytic activity in light hydrocarbon oxidation is shown to correlate with the RedO*x* properties of PdPt–MnO_x–Al_2O_3 catalysts and the Pt–Pd particle size. The non-additive increase in the catalytic activity of bimetallic catalyst is suggested to connect with a formation of nanoscale PdO–PtO_x particles on the surface of Mn_3O_4 and a modification of alumina structure by Mn^{3+} and PtPd clusters.

1. Introduction

The three way catalysts (TWC) for catalytic converters of diesel engines usually contain noble metals—Pt and Pd, which have high catalytic activity in CO and hydrocarbon oxidation [1–3], and Rh, which has high activity in nitrogen oxides removal [2,3]. In the last decade, there has been a trend of progressive alteration of the preferred loadings of Pt or Pd, depending mostly on the market value dynamics of these metals. The catalytic systems with a low noble metal (Pt, Pd, Rh) content and especially their combinations with transition metal oxides are shown to be an attractive option for TWC perfecting [1,4]. Such combinations of noble metals with suitable metal oxides are of the greatest interest for close-coupled converters operated at high temperatures [4]. There is also a great number of data on non-additive increase in the catalytic activity of noble metals combination with transition metal oxides in the oxidation of carbon monoxide and hydrocarbons [4–11].

In our previous papers [4,10], we demonstrated the synergetic effect of Pt and manganese oxides, which allows a decrease in the Pt loading from 1.00–1.75 g/L to 0.70 g/L in the monolithic catalyst for diesel engine exhaust treatment. The Pt–MnO_x–Al_2O_3 catalytic composition with a 0.70 g/L Pt loading provides high activity in low temperature oxidation of CO and light hydrocarbons and demonstrates high thermal stability (up to 900 °C). However, such Pt loading is quite high in commercial terms. Therefore, we attempted to reduce the platinum content in Pt–MnO_x–Al_2O_3 monolith by replacing a part of Pt with Pd.

Here, we are reporting our systematic study on the effect of Pd addition into Pt–MnO_x–Al_2O_3 monolithic catalysts with a 0.17 g/L Pt loading on their catalytic activity and stability in hydrocarbon (butane and a mixture of propane with propene) and CO oxidation. The catalyst preparation approach emphasized variation of a Pd precursor, Pd content, and total loading of noble metals. The catalysts were studied before and after aging in dry and wet air at

* Corresponding author.
E-mail address: yashnik@catalysis.ru (S.A. Yashnik).

http://dx.doi.org/10.1016/j.apcatb.2015.12.017
0926-3373/

750 °C. We are discussing also the RedO*x* properties, particle size and morphology, and interaction of nanoscale Pt/Pd particles with Mn-modified alumina in order to explain a positive effect of Pd on catalytic behavior of Pt–Mn–alumina catalyst.

2. Experimental

2.1. Catalyst preparation

The route of washcoating a layer on cordierite monolithic substrate has been presented in [10]. The washcoated cordierite samples were prepared by immersion of cordierite monoliths (Corning, cell density of 400 cpsi) in a slurry containing 80% of γ-Al_2O_3 powder and 20% of a binding agent made from aluminum hydroxide with pseudoboehmite structure, with subsequent treatment at 500 °C. The washcoat loading was about 15 ± 1 wt.% of the total support weight. Then the γ-Al_2O_3 washcoat layer was impregnated with manganese nitrate and treated at 900 °C. Mn loading was 3.61–3.65 wt.% of the washcoat layer weight. Their XRD composition and textural properties are presented in Table 1.

Pt and/or Pd were supported by wetness impregnation of cordierite monolith washcoated by MnO_x–Al_2O_3 with solutions of Pt and Pd precursors, with subsequent treatment in air flow at 600 °C. The solutions of hexachloroplatinic acid or platinum dinitrodiamine were used as Pt precursors. The solutions of tetrachloropalladic acid, palladium acetate, palladium nitrate and tetraaminepalladium nitrate were used as Pd precursors. Total Pd-Pt loading was varied from 0 to 0.70 g/L (from 0 to 0.11 wt.%). The resulting noble metal loadings determined by X-ray fluorescence spectroscopy are listed in Tables 2–4 .

The samples are designated as *S*-*n*Pt*Z*-*m*Pd*Y*, where *S* is the composition of washcoated layer (MA —MnO_x–Al_2O_3; A—Al_2O_3), *n* and *m* are the Pt and Pd loadings in g/ft^3, *Z* is the Pt precursor (PtClA—hexachloroplatinic acid, PtNA – platinum dinitrodiamine), *Y* is the Pd precursor (PdClA—tetrachloropalladic acid, PdN—palladium nitrate, PdA—palladium acetate, and PdNN—tetraaminepalladium nitrate).

2.2. Catalytic activity testing

Hydrocarbon chemical composition of the diesel exhaust gases is quite complicated and includes mostly C_3–C_{18} alkanes (7–17 ppm), C_2–C_5 alkenes, dienes, alkynes (12–27 ppm), light aromatics of benzene family (2–3 ppm), C_{16}–C_{23} heavy alkanes adsorbed on soot (<2 ppm), and others [12]. Alkane ability to be oxidized over Pt and PtRh catalysts was shown [12,13] to strongly depend on their structure. For example, alkane oxidability appreciably increases with chain length from methane to C_{10}, and a light-off temperature for C_{10}–C_{20} alkanes are very close [12,13]. Light alkenes are more reactive than light alkanes [12]. The branched alkanes, such as 2-methyl propane and isooctane, and cyclohexane have light-off temperatures similar to *n*-butane [13]. The presence of alkynes inhibits the oxidation of alkanes and CO and their oxidation starts only after alkynes are converted [13]. So, propane/propene and butane were chosen by us as model hydrocarbon of diesel exhaust gases. We believe that the catalyst oxidizing C_3–C_4 hydrocarbons is active in oxidation of C_5–C_{18} alkanes and C_2–C_5 alkenes/alkynes.

To optimize the composition of a diesel oxidation catalyst, the MnO_x–Al_2O_3 and Pd,Pt-modified MnO_x–Al_2O_3 washcoated monoliths were tested in butane oxidation. Their catalytic activity in the butane oxidation reaction was studied using a quartz flow reactor in the temperature range 200–700 °C at a space velocity 12,000 h^{-1}. The reactor was placed into a furnace. For the control of temperature, the K-type thermocouple inserted in the catalyst bed was used. The composition of the gas mixture was 0.1 vol.% butane in air. Samples of a monolithic catalyst of 1 cm^3 volume were used in the activity test experiments.

The catalytic activity of the most interesting samples was tested in test runs with a mixture of propane/propene (100/200 ppm), CO (1900 ppm), NO (300 ppm), O_2 (14.6 vol.%), CO_2 (2.5 vol%), H_2O (3.9 vol%), and N_2 (balance), in two heating/cooling cycles from 25 to 400 °C. Except for hydrocarbons and SO_2, the mentioned composition of the reaction mixture was similar to the composition of the diesel exhaust gases [12], therefore we conditionally called a test as DIESEL test. For DIESEL test, two cylindrical samples of the monolithic catalyst 25 mm in diameter and 75 mm in length were used at a space velocity 67,000 h^{-1}. The catalytic activity was characterized by an average value (for two parallel samples) of the 50%, 75% or 90% conversion temperature of hydrocarbons (HC), CO, and NO in the second heating cycle, and by the steady-state value of HC, CO, and NO conversion at 400 °C.

Active regeneration of diesel particulate filters by soot burning requires the diesel oxidation catalyst to withstand a high temperature effect. During this regeneration, catalyst temperatures can rise up to 750 °C [14]. Since a sintering of the active component is a key factor of catalyst deactivation, the protocols of "thermal aging" and "hydrothermal aging" effectively simulate diesel oxidation catalysts performance deterioration during vehicle use [14–16]. For evaluation of thermal stability, the samples were aged in a flow of dry air at 750 °C for 7 h. The most thermostable catalyst was aged additionally in dry air at 750 °C for 7 h, and then in wet air (10 vol.%) at 750 °C for 7 h. The aged samples were examined in DIESEL tests at indicated above conditions.

2.3. Catalyst characterization

2.3.1. The X-ray diffraction

(XRD) analysis was carried out using an HZG-4C diffractrometer (Fre/Berger Prazisionmechanik) with monochromatic CuKα (λ = 1.5418 Å) irradiation. The phase compositions were determined using diffraction patterns recorded in the 2θ range 10–70° with 1°/min scanning rate. The observed diffraction patterns were identified using the JCPDS database (PCPDF Win. Ver. 1.30, JCPDS ICDD, Swarthmore, PA, USA, 1997).

2.3.2. Transmission electron microscope (TEM) and high-resolution transmission electron microscope

(HRTEM) images were obtained using a JEM-2010 electron microscope (JEOL, Japan) with a lattice-fringe resolution of 0.14 nm at an accelerating voltage of 200 kV. The high-resolution images of periodic structures were analyzed by the Fourier method. Local energy-dispersive X-ray analysis (EDX) was carried out using an EDX spectrometer (EDAX Co.) fitted with a Si (Li) detector with the resolution of 130 eV. The samples for the HRTEM study were prepared on a perforated carbon film mounted on a copper grid.

2.3.3. Temperature-programmed reduction

(H_2-TPR) experiments were carried out using a hydrogen-argon mixture (10 vol.% H_2) with the flow rate of 40 mL/min in a laboratory instrument equipped with a thermal conductivity detector. The temperature was raised from 0 to 900 °C at 10 °C/min rate. Before the TPR experiments, the samples were first pretreated in oxygen at 500 °C for 30 min and cooled to room temperature, and then flushed with an Ar flow. The weight of the samples was 100 mg and the particle size was 250–500 μm. Water produced during the TPR experiment was removed using a cold trap at −70 °C. The hydrogen consumption was calibrated against the reduction of CuO (Reachem, very-high-purity) under similar conditions, assuming a complete one-step CuO reduction to zero-valent copper.

Table 1
XRD composition and textural properties of manganese-alumina washcoat pretreated at different conditions.

XRD composition	Pretreatment conditions	Surface area, S_{BET}, m^2/g	Pore volume, V_Σ, cm^3/g	Average pore radius, nm
Series MA:				
1. Mn^{3+}-γ^*-Al_2O_3 (a—7.94 –7.95 Å) Al^{3+}-β-Mn_3O_4 (a—8.05–8.15 Å)	Fresh, 900 °C/4 h	105	0.40	15.3
2. Mn^{3+}-γ^*-Al_2O_3 (a—7.94–7.95 Å) Al^{3+}-β-Mn_3O_4 (a—8.05–8.15 Å)	Aged, 750 °C/7 h dry air	107	0.40	15.0
3. Mn^{3+}-γ^*-Al_2O_3 (a—7.94–7.95 Å) Al^{3+}-β-Mn_3O_4 (a —8.05–8.15 Å)	Aged, 750 °C/7 h wet air	103	0.39	15.0

Table 2
Chemical composition of monolithic catalysts washcoated by Pt–MnO_x–Al_2O_3 and Pd–MnO_x–Al_2O_3. Effect of noble metal precursors on their catalytic properties in butane oxidation.

No.	Sample[a]	Chemical composition[b]				Temperature of X% C_4H_{10} conversion, °C		
		Pt, g/L	Pt, wt.%	Pd, g/L	Pd, wt.%	$T_{20\%}$	$T_{50\%}$	$T_{90\%}$
1.	MA-0	–	–	–	–	330	385	550
2.	MA-5PtClA	0.17	0.03	–	–	315	355	500
3.	MA-10PtClA	0.35	0.06	–	–	285	340	485
4.	MA-5PtNA	0.17	0.03	–	–	285	345	445
5.	MA-10PtNA	0.35	0.06	–	–	270	315	425
6.	MA-15PtNA	0.52	0.09	–	–	265	310	425
7.	MA-10PdClA	–	–	0.35	0.06	295	345	407
8.	MA-10PdN	–	–	0.35	0.06	295	336	400
9.	MA-10PdA	–	–	0.35	0.06	275	317	370
10.	MA-10PdNN	–	–	0.35	0.06	307	350	417
11.	MA-15PdN	–	–	0.52	0.09	290	330	395

[a] The samples denoted as MA-nPtZ and MA-mPdY, where MA is the composition of washcoated layer MnO_x–Al_2O_3, n and m are the Pt and Pd loading in g/ft^3, PtZ is the Pt precursor (PtClA—hexachloroplatinic acid, PtNA—platinum dinitrodiamine), PdY is the Pd precursor (PdClA—tetrachloropalladic acid, PdN—palladium nitrate, PdA—palladium acetate, PdNN—tetraaminepalladium nitrate).
[b] Mn loading in all samples is 3.61–3.65 wt.% of the washcoat layer weight.

Table 3
Chemical composition of monolithic catalysts washcoated by Pd–Pt–MnO_x–Al_2O_3 and Pd–Pt–Al_2O_3. Effect of loading and precursors of Pd on catalytic properties in butane oxidation of the ex-hexachloroplatinic-acid Pt–MnO_x–Al_2O_3 catalysts.

N	Sample[a]	Chemical composition[b]				Temperature of X% C_4H_{10} conversion, °C		
		Pt,g/L	Pt,wt.%	Pd,g/L	Pd, wt.%	$T_{20\%}$	$T_{50\%}$	$T_{90\%}$
1.	MA-5PtClA-10PdClA	0.17	0.03	0.35	0.06	272	308	380
2.	MA-5PtClA-10PdN	0.17	0.03	0.35	0.06	270	292	360
3.	MA-5PtClA-10PdA	0.17	0.03	0.35	0.06	272	308	360
4.	MA-5PtClA-10PdNN	0.17	0.03	0.35	0.06	280	324	410
5.	MA-10PtClA-5PdN	0.35	0.06	0.17	0.03	250	300	400
6.	A-5PtClA-10PdClA	0.17	0.03	0.35	0.06	300	360	510

[a] The samples denoted as S-nPtZ-mPdY, where S is the composition of washcoated layer (MA—MnO_x–Al_2O_3; A—Al_2O_3), n and m are the Pt and Pd loading in g/ft^3, PtClA is hexachloroplatinic acid used as Pt precursor, PdY is the Pd precursor (PdClA—tetrachloropalladic acid, PdN—palladium nitrate, PdA—palladium acetate, PdNN—tetraaminepalladium nitrate).
[b] Mn loading in all samples is 3.61–3.65 wt.% of the washcoat layer weight.

Table 4
Chemical composition of monolithic catalysts washcoated by Pd–Pt–MnO_x–Al_2O_3 and Pd–Pt–Al_2O_3. Effect of loading and precursors of Pd on catalytic properties in butane oxidation of the ex-platinum-dinitrodiamine Pt–MnO_x–Al_2O_3 catalysts.

N	Sample[a]	Chemical composition[b]				Temperature of X% C_4H_{10} conversion, °C		
		Pt, g/	Pt, wt.%	Pd, g/L	Pd, wt.%	$T_{20\%}$	$T_{50\%}$	$T_{90\%}$
1.	MA-5PtNA-10PdClA	0.17	0.03	0.35	0.06	270	307	425
2.	MA-5PtNA-10PdN	0.17	0.03	0.35	0.06	260	285	335
3.	MA-5PtNA-10PdA	0.17	0.03	0.35	0.06	250	282	345
4.	MA-5PtNA-10PdNN	0.17	0.03	0.35	0.06	260	300	395
5.	MA-5PtNA -5PdN	0.17	0.03	0.17	0.03	265	290	335
6.	MA-5PtNA-15PdN	0.17	0.03	0.52	0.09	245	280	340
7.	MA-5PtNA-20PdN	0.17	0.03	0.70	0.12	245	278	345
8.	MA-10PtNA-5PdN	0.35	0.06	0.17	0.03	244	280	362
9.	A-5PtNA-10PdClA	0.17	0.03	0.35	0.06	295	355	500
10.	A-5PtNA-10PdN	0.17	0.03	0.35	0.06	290	350	500

[a] The samples denoted as S-nPtZ-mPdY, where S is the composition of washcoated layer (MA—MnO_x–Al_2O_3; A—Al_2O_3), n and m are the Pt and Pd loading in g/ft^3, PtNA is platinum dinitrodiamine used as the Pt precursor, PdY is the Pd precursor (PdClA—tetrachloropalladic acid, PdN—palladium nitrate, PdA—palladium acetate, PdNN—tetraaminepalladium nitrate).
[b] Mn loading in all samples is 3.61–3.65 wt.% of the washcoat layer weight.

2.3.4. Specific surface areas

(S_{BET}, m^2/g), total pore volumes (V_Σ, cm^3/g), and mesopore size were determined by thermal desorption of nitrogen using an ASAP-2400 instrument.

3. Results and discussion

3.1. Catalytic activity in butane oxidation

The catalytic activity data in butane oxidation on monolithic catalysts washcoated by MnO_x–Al_2O_3, Pt–MnO_x–Al_2O_3, and Pd–MnO_x–Al_2O_3 are presented in Table 2. One can see, the catalytic activity of washcoated monometallic Pd–MnO_x–Al_2O_3 catalysts depends on a noble metal precursor, similar to Pt–MnO_x–Al_2O_3 catalysts [10]. At a Pd loading equal to 0.35 g/L, the catalytic activity in butane oxidation was in an ascending order in a series of Pd precursors: $Pd(NH_3)_4(NO_3)_2 < H_2PdCl_4 < Pd(NO_3)_2 < Pd(CH_3COO)_2$ (Table 2, samples 7–11).

At equal loading of noble metals, the monometallic Pt–MnO_x–Al_2O_3 washcoated catalysts are more active in low-temperature butane oxidation than Pd–MnO_x–Al_2O_3 (Table 2, $T_{20\%}$). The Pt–MnO_x–Al_2O_3 and Pd–MnO_x–Al_2O_3 monoliths with noble metal loading 0.35 g/L (or 0.06 wt.%) provided 20% conversion of butane at 270–285 °C [10] and 295–307 °C (Table 2, samples N 3, 5 and 7–11), respectively. But, Pd–MnO_x–Al_2O_3 catalysts ensure total butane oxidation at lower temperature compared with Pt–MnO_x–Al_2O_3 samples (Table 2, $T_{90\%}$). Their temperature of 90% conversion of butane is 407 and 485 °C, respectively, for monometallic ex-chloride Pd–MnO_x–Al_2O_3 (Table 2, Sample 7) and Pt–MnO_x–Al_2O_3 (Table 2, Sample 3) catalysts with noble metal loading 0.35 g/L. Both of them are more active than MnO_x–Al_2O_3 washcoated catalyst (Table 2, Sample 1).

Note, Pt–MnO_x–Al_2O_3 catalysts have demonstrated the synergetic effect in catalytic activity of Pt–Al_2O_3 and MnO_x–Al_2O_3 in the butane oxidation and in the DIESEL test [10]. The synergetic effect is strongly dependent on Pt precursors, and it was more noticeable for platinum dinitrodiamine as compared to hexachloroplatinic acid and others [10]. The same result is shown by MA-10PtNA and MA-10PtClA catalysts, whose temperature of 50% conversion was 315 and 340 °C, respectively (Table 2, Sample 5 and 3). So, here platinum dinitrodiamine was used for the preparation of bimetallic Pt-Pd monolithic catalysts with MnO_x–Al_2O_3 washcoat; however, the Pt content was decreased from 0.70 g/L [10] to 0.17 g/L. For comparison, hexachloroplatinic acid was also used for the preparation of bimetallic Pt–Pd catalysts. The data of 20, 50 and 90% butane conversion temperature for bimetallic Pt–Pd–MnO_x–Al_2O_3 monolithic catalysts prepared from different Pt and Pd precursors are presented in Tables 3 and 4.

The analysis of catalytic activity in butane oxidation revealed three preliminary conclusions.

First, the addition of 0.35 g Pd per liter to the washcoated Pt–MnO_x–Al_2O_3 monolithic catalysts containing 0.17 g/L of Pt significantly improves the catalytic performance of the catalysts in butane oxidation. Besides, the increase in the catalytic activity of bimetallic Pt–Pd–MnO_x–Al_2O_3 catalysts is higher than the sum of the activities of 0.17 g/L Pt and 0.35 g/L Pd catalysts. For example, the temperatures of 50% butane conversion ($T_{50\%}$) are 285 and near 336–345 °C, respectively, for the MA-5PtNA-10PdN (Table 4, Sample 2) and the catalytic bed base on MA-5PtNA with MA-10PdN (Table 2, Sample 4 and 8). On the other hand, the catalytic activity of bimetallic Pt–Pd–MnO_x–Al_2O_3 catalyst is also higher than those of Pt–MnO_x–Al_2O_3 and Pd–MnO_x–Al_2O_3 with the individual noble metal loadings equal to the sum of loadings in the bimetallic catalyst, 0.52 g/L. Thus, $T_{50\%}$ are 285, 310, and 330 °C, respectively, for the MA-5PtNA-10PdN (Table 4, Sample 2), MA-15PtNA (Table 2, Sample 6) and MA-15PdN (Table 2, Sample 11) samples with similar noble metal loadings.

Second, there is another synergetic increase in the catalytic activity in Pt–Pd–MnO_x–Al_2O_3 as compared to noble bimetallic catalyst Pt–Pd–Al_2O_3 (series A, Table 4) and oxide catalyst MnO_x–Al_2O_3 (series MA-0). So, the $T_{50\%}$ is 285, 350, and 385 °C for the MA-5PtNA-10PdN (Table 4, Sample 2), A-5PtNA-10PdN (Table 4, Sample 10), and MA-0 (Table 2, sample 1) monolithic catalysts, respectively.

Third, these two synergetic effects are observed for all Pt and Pd precursors used in the study. They are more pronounced for platinum dinitrodiamine (Table 4, samples 1–4) compared to chloroplatinic acid (Table 3, sample 1–4), and for palladium nitrate (Table 4, sample 2) and palladium acetate (Table 4, sample 3) compared to chloropalladic acid (Table 4, sample 1). For bimetallic Pt–Pd–MnO_x–Al_2O_3 catalysts with a Pd loading equal to 0.35 g/L, the activity in butane oxidation ascended in the order: $H_2PdCl_4 \sim Pd(NH_3)_4(NO_3)_2 < Pd(NO_3)_2 \sim Pd(CH_3COO)_2$. This order of the activity dependence on Pd precursor has an analogy to that observed for monometallic Pd–MnO_x–Al_2O_3 catalysts (Table 2, samples 7–11).

When the bimetallic Pt–Pd–MnO_x–Al_2O_3 catalysts were prepared using platinum dinitrodiamine and palladium nitrate, their catalytic activity in butane oxidation increased with an increase in the Pd loading up to 0.52 g/L, and further was nearly constant up to 0.70 g/L (Table 4, samples 2, 5, 6, 7). A similar decrease in $T_{50\%}$ with Pd loading was observed for another pair of Pd and Pt precursors.

With the same pair of precursors and a constant total noble metal content, the catalytic activity of bimetallic Pt–Pd–MnO_x–Al_2O_3 catalysts also depends on the atomic ratio of Pt/Pd. The higher is the atomic Pt/Pd ratio of the catalyst, the lower is the light-off temperature ($T_{20\%}$). At a total noble metal loading of 0.52 g/L, $T_{20\%}$ in butane oxidation was 245–250 °C for Pt–Pd–MnO_x–Al_2O_3 with atomic Pt/Pd equal to 1 (Table 3, sample 5 and Table 4, sample 8); it is 20 °C lower than for the catalyst with Pt/Pd = 0.25 (Table 3, sample 2 and Table 4, sample 2). This result correlates well with a higher catalytic activity of Pt–MnO_x–Al_2O_3 in comparison with that of Pd–MnO_x–Al_2O_3 observed in the low-temperature butane oxidation as discussed above. Although, at moderate butane conversion, the influence of the Pt/Pd ratio on the activity is smoothed; and at a higher butane conversion, it disappears. There are the Pd species are more active than Pt.

3.2. Catalytic activity in DIESEL test

Diesel oxidation catalysts must secure simultaneous transformation of hydrocarbons, CO and NO to nontoxic compounds: CO_2, H_2O and N_2. Components of diesel exhaust gas have mutual impact on oxidation and reduction of each other [13–20], the most strongly this effect is shown on transformations of NO [13,17–20].

The bimetallic catalyst MA-5PtNA-15PdN was used as an example to study the influence of reaction mixture composition on route of NO transformation. The results are shown on Figs. 1 and 2. When the reaction mixture contained 300 ppm NO and 10 vol.% O_2 in argon, the catalyst efficiently oxidized NO to NO_2. The maximum conversion of NO to NO_2 was about 45% at 350–410 °C and GHSV 67,000 h^{-1} (Fig. 1, curve 2). At increasing temperature above 410 °C, the conversion of NO to NO_2 was limited to thermodynamic equilibrium [17]. NO oxidation rate is strongly dependent on the oxygen concentration, decreasing with a diminution of oxygen concentration in the reaction mixture. NO conversion to NO_2 did not exceed 30% for 3 vol.% O_2 (Fig. 1, curve 4). High activity of the bimetallic catalyst MA-5PtNA-15PdN in NO oxidation agrees with the well-known ability of the mono- and the bimetallic Pt-containing catalysts oxidize NO to NO_2 [17–20] or N_2O [20] as well as with promoter effect of MnOx on this reaction [21,22].

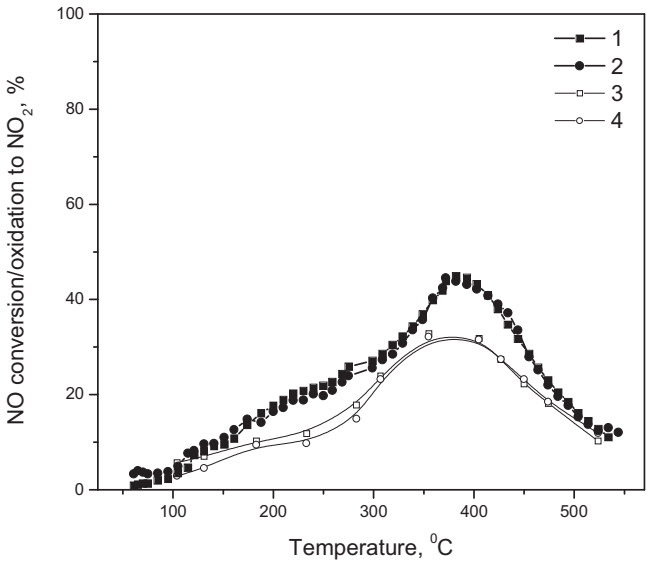

Fig. 1. NO conversion (1,3) and NO oxidation to NO_2 (2,4) over catalyst MA-5PtNA-15PdN versus temperature. Gas mixture of 300 ppm NO, 3 vol.% (3,4) or 10 vol.% (1,2) O_2 in Ar. GHSV was 67,000 h^{-1}.

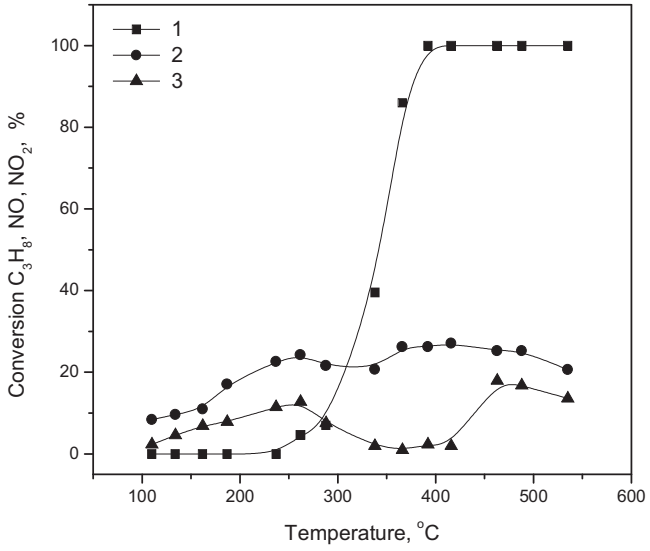

Fig. 2. C_3H_8 conversion (1), NO conversion (*2*) and NO oxidation to NO_2 (*3*) over catalyst MA-5PtNA-15PdN versus temperature. Gas mixture of 300 ppm NO, 1700 ppm C_3H_8, 10 vol.% O_2 in Ar. GHSV was 67,000 h^{-1}.

On the other part, NO oxidation to NO_2 over noble metal supported catalysts is inhibited by hydrocarbons [13,18–24] and CO [23–25]. For example, the NO conversion over catalyst MA-5PtNA-15PdN decreased from 45% to 23–27% after addition of 600 or 1700 ppm of propane in the reaction mixture, consisting from 300 ppm NO and 10 vol.% O_2 in Ar (Fig. 2, curve 2). 11–13% of NO is oxidized to NO_2 (Fig. 1, curve 3) and 11% of NO is reduced to N_2 at a temperature range of 225–260 °C, where the propane conversion was not less than 5% (Fig. 1, curve 1). NO_2 was formed in trace amounts (<2–5 ppm) at temperatures 340–420 °C, at which C_3H_8 conversion was varied from 40 to 99%, although there was 20–27% of NO conversion. When the temperature was above the temperature for 99% of C_3H_8 conversion (>420 °C), NO_2 was again observed in the reaction products. Other authors also pointed to the close correlation between the NO reduction and hydrocarbons oxidation [20,24]. Therefore, we can conclude that both the selective catalytic reduction of NO or NO_2 with propane to N_2 and the oxidation of NO to NO_2 occur over MA-5PtNA-10PdN catalyst. In the real diesel exhaust control system, containing CO and C_2–C_5 alkenes, the selective NO reduction into N_2 will be promoted because alkenes are more effective in the DeNO*x* over Pt-containing catalyst than *n*-paraffins and aromatics [13,20,24], and their activity increases with increasing carbon number [20,24]. Note that formation of NO_2 is not a lack of the diesel oxidation catalyst, because NO_2 is used downstream to improve a performance of the system of the diesel exhausts control, for example, in passive regeneration of diesel particulate filter [26], the NO*x* storage reduction catalyst [27,28] and the selective reduction catalyst [27,29,30].

The relevance of a precursor and noble metal loading for catalytic performance of washcoated Pt–Pd–MnO_x–Al_2O_3 monolithic catalysts is also confirmed by DIESEL test experiments. The results of the DIESEL tests are presented in Tables 5 and 6 (as a function of Pd precursor) and in Figs. 3 and 4 (as a function of Pd loading).

At an equal loading of noble metals, the fresh Pt–MnO_x–Al_2O_3 and Pd–MnO_x–Al_2O_3 monometallic monolithic catalysts have similar catalytic properties, but the first catalyst is more thermostable than the second one. So, at a 0.70 g/L noble metal loading, the temperatures of 50% conversion of CH and CO were, respectively, 247 and 228 °C on Pt–MnO_x–Al_2O_3 monolith and 259 and 230 °C on Pd–MnO_x–Al_2O_3 (Table 5, Samples 3 and 4). While, after aging at 750 °C in dry air, the aged Pt–MnO_x–Al_2O_3 catalysts (Table 5, samples 2 and 3) had lower temperatures of 50% conversion of CH, CO and NO. They were $_x$ equal to 205–209, 171–192, and 215–217 °C, respectively, which were about 70–90 °C lower than that for the aged Pd–MnO_x–Al_2O_3 catalyst (Table 5, sample 4). Data of NO conversion on the aged MnO_x–Al_2O_3 (Table 5, sample 1) and Pd–MnO_x–Al_2O_3 (Table 5, sample 4) catalysts at 400 °C were rather low, 19 and 42%, respectively, instead of 57–58% on Pt–MnO_x–Al_2O_3 monolith (Table 5, samples 2 and 3).

The bimetallic Pt–Pd–MnO_x–Al_2O_3 catalysts were superior in DIESEL test to monometallic monoliths Pt–MnO_x–Al_2O_3 and Pd–MnO_x–Al_2O_3, even at a lower total content of noble metal. Thus, when Pd was added only in 0.17 g/L to Pt–MnO_x–Al_2O_3 catalyst, the temperatures of 50% CH and CO conversion on fresh monolith dramatically decreased from 295–303 to 183–205 °C and from 276–288 to 180–199 °C, respectively (Fig. 3a and b). At 400 °C, CH and CO conversions on the fresh bimetallic MA-5PtNA-5PdN sample were 97.1–98.6% and 99.9%, respectively (Fig. 4a and b). For comparison, CH conversion on monometallic MA-5PtNA reached only 71.5% (Fig. 4a). Similar trends were observed for the aged catalysts.

The catalytic behavior of the bimetallic Pd–Pt–MnO_x–Al_2O_3 sample improves with further increasing the Pd loading up to 0.35 g/L, which is characterized by a decrease in the temperature of 50% conversion of HC, CO, and NO (Fig. 3) and an increase in the hydrocarbon, CO and NO conversion at 400 °C (Fig. 4). At the same noble metal loadings, the bimetallic sample MA-5PtNA-15PdN, that was prepared from platinum dinitrodiamine and palladium nitrate, possessed a lower temperature of 50% conversion of HC, CO, and NO compared with monometallic MA-20PtNA and MA-20PdN catalysts prepared from the same precursors of the noble metal.

The higher catalytic activity of the bimetallic Pd–Pt–MnO_x–Al_2O_3 catalyst compared to monometallic Pd–MnO_x–Al_2O_3 and Pt–MnO_x–Al_2O_3 monoliths was found for all three Pd precursors that had been chosen for the work: palladium nitrate, tetraaminepalladium nitrate, and chloropalladic acid. The sample containing 0.17 g Pt/L–0.35 g Pd/L and prepared using $Pt(NH_3)_2(NO_2)_2$ and $Pd(NO_3)_2$ (Table 6, sample 2) is slightly more active in the reaction of HC and CO oxidation at 400 °C than the samples prepared using $Pt(NH_3)_2(NO_2)_2$ with $Pd(NH_3)_4(NO_3)_2$ or H_2PdCl_4 (Table 6, samples 1, 3). However, the former shows smaller activity in the low-temperature oxidation of hydrocarbons and CO than the other two catalysts. The former provided 50%

Table 5
DIESEL test results for initial and aged Pt–MnO_x–Al_2O_3 and Pd–MnO_x–Al_2O_3 monolithic catalysts.

No.	Samples*	Temperature of X% conversion, °C						Conversion at 400 °C, %		
		CH		CO		NO		CH	CO	NO
		T_{50}	T_{75}	T_{50}	T_{90}	T_{50}	max $X(T_{max})$			
Initial catalyst**										
1	MA-0	–	–	–	–	–	–	28.7	20.8	10.3
2	MA-20PtClA	284	393	273	288	–	32(393)	81.5	99.7	40.4
3	MA-20PtNA	247	368	228	247	–	49(368)	84.4	99.8	43.4
4	MA-20PdN	259	326	230	257	–	42(373)	97.2	99.9	47.8
Aged catalyst (at 750 °C, 7 h, in dry air)										
1	MA-0	–	–	384	–	–	21(384)	45.5	66.1	19.0
2	MA-20PtClA	205	390	171	205	215	62(390)	77.4	99.8	58.7
3	MA-20PtNA	209	380	192	210	217	63(380)	78.5	99.8	56.9
4	MA-20PdN	293	374	260	299	–	44(374)	83.8	99.1	42.2

* The samples denoted as MA-20PtZ and MA-20PdY, where MA is the MnO_x–Al_2O_3 composition of washcoated layer, 20 is the Pt and Pd loading in g/ft^3, PtZ is the Pt precursor (PtClA—hexachloroplatinic acid, PtNA—platinum dinitrodiamine), PdY is the Pd precursor (PdN—palladium nitrate).
** Mn loading in all samples is 3.61–3.65 wt.% of the washcoat layer weight.

Table 6
Effect of Pd precursors on DIESEL test results for initial and aged Pt–Pd–MnO_x–Al_2O_3 monolithic catalysts.

No.	Samples*	Temperature of X% conversion, °C						Conversion at 400 °C, %		
		CH		CO		NO		CH	CO	NO
		T_{50}	T_{75}	T_{50}	T_{90}	T_{50}	max $X(T_{max})$			
Initial catalyst**										
1	MA-5PtNA-10PdClA	192	364	183	194	–	12(364)	87.4	99.9	20.4
		192	329	180	197	–	15(355)	91.6	98.2	23.0
2	MA-5PtNA-10PdN	218	289	211	220	356	51(356)	99.6	99.9	59.6
		207	292	200	208	389	55(400)	99.4	99.9	55.0
3	MA-5PtNA-10PdNN	195	293	195	197	255	54(347)	98.6	99.9	53.2
		208	291	205	208	359	53(360)	98.7	99.9	52.2
Aged catalyst (at 750 °C, 7 h, in dry air)										
1	MA-5PtNA-10PdClA	189	329	176	197	244	57(329)	91.6	98.2	47.8
		183	334	175	183	291	52(299)	89.7	98.7	50.2
2	MA-5PtNA-10PdN	178	287	174	179	245	63(337)	97.9	99.9	54.3
		197	293	178	182	257	63(380)	96.5	99.9	58.5
3	MA-5PtNA-10PdNN	209	352	196	212	327	51(327)	88.6	99.8	52.9
		214	400	203	214	–	50(360)	75.1	99.9	47.7

* The samples denoted as MA-5PtNA-10PdY, where MA is the MnO_x–Al_2O_3 composition of washcoated layer, 5 and 10 are the Pt and Pd loading in g/ft^3, respectively; PtNA is platinum dinitrodiamine used as the Pt precursor, PdY is the Pd precursor (PdClA—tetrachloropalladic acid, PdN—palladium nitrate, PdNN—tetraaminepalladium nitrate).
** Mn loading in all samples is 3.61–3.65nwt.% of the washcoat layer weight.

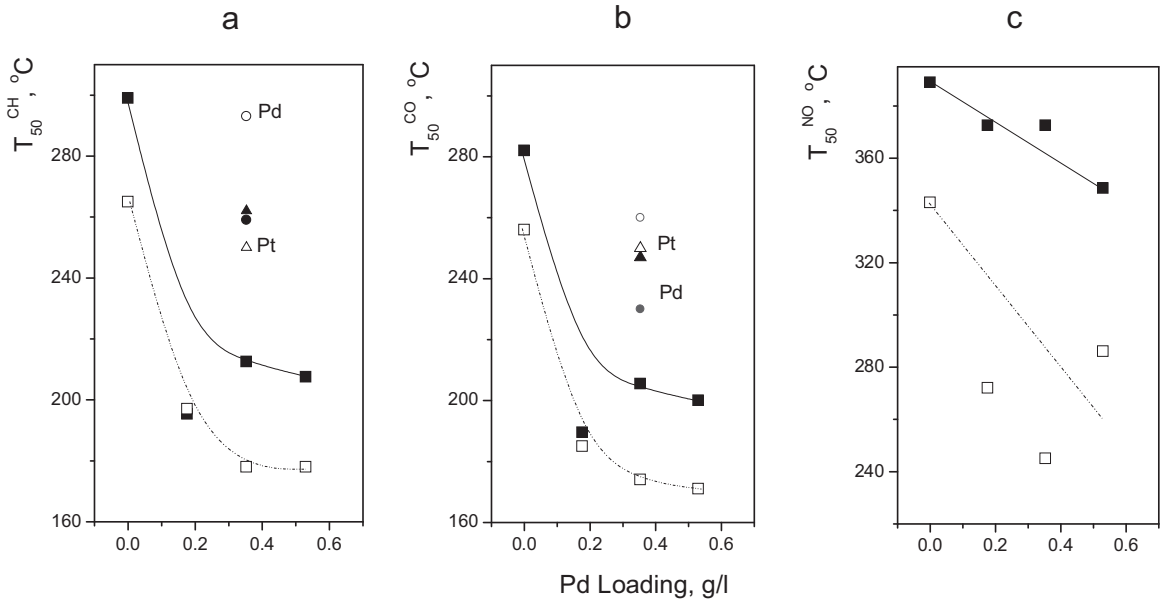

Fig. 3. Temperature of 50% conversion of CH (a), CO (b), and NO (c) for Pd–Pt–MnO_x–Al_2O_3 (■,□) monolithic catalysts prepared from $Pt(NH_3)_2(NO_2)_2$ and $Pd(NO_3)_2$ vs. Pd loading, initial (close symbols, ■) and aged (open symbols, □) at 750 °C in dry air. The Pt loading in Pd–Pt–MnO_x–Al_2O_3 catalysts is 0.17 g/L. The data for Pd–MnO_x–Al_2O_3 (●,○) and Pt–MnO_x–Al_2O_3 (▲,△) monolithic catalysts are presented for comparison. The Pd and Pt content in Pd–MnO_x–Al_2O_3 and Pt–MnO_x–Al_2O_3 catalysts is 0.35 g/L.

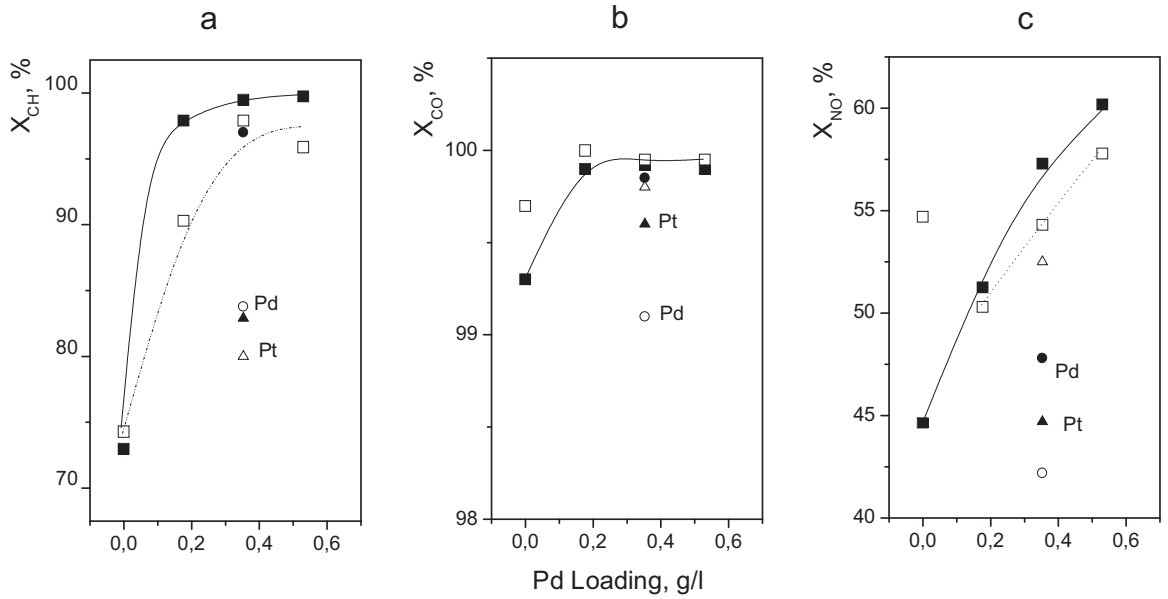

Fig. 4. Conversion of CH (a), CO (b) and NO (c) at 400 °C for Pd–Pt–MnO_x–Al_2O_3 (■,□) monolithic catalysts prepared from $Pt(NH_3)_2(NO_2)_2$ and $Pd(NO_3)_2$ vs. Pd loading, initial (close symbols, ■) and aged (open symbols, □) at 750 °C in air. The Pt loading in Pd–Pt–MnO_x–Al_2O_3 catalysts is 0.17 g/L. The data for Pd–MnO_x–Al_2O_3 (●,○) and Pt–MnO_x–Al_2O_3 (▲,△) monolithic catalysts are presented for comparison. The Pd and Pt content in Pd–MnO_x–Al_2O_3 and Pt–MnO_x–Al_2O_3 catalysts is 0.35 g/L.

conversion of CO and CH at somewhat higher temperatures, 200–218 °C instead of 180–195 °C.

So, the bimetallic Pd–Pt–MnO_x–Al_2O_3 catalysts are characterized by the synergetic effect in catalytic activity. Advantages of the synergetic effects of Pt, Pd and manganese oxides observed in the light hydrocarbon and CO oxidation resulted in the development of a new diesel exhaust catalyst with the Pd loading of 0.35 g/L and Pt loading as low as 0.17 g/L instead of the traditional amount of 1.0–1.75 g/L. But the oxidation catalyst is acceptable for the diesel exhaust control when it is not only active in the oxidation of CO and hydrocarbons, but its behavior is stable in the real diesel exhaust for at least 1000 h.

3.3. *Thermal aging of bimetallic Pd–Pt–MnO_x–Al_2O_3 catalysts*

The catalyst is under a high-temperature influence of diesel vehicle exhaust; as a result, a thermal effect is considered to be the main reason of its rapid deactivation and loss of catalytic activity. Our long term aging experiments have elucidated a very important phenomenon testifying that thermal aging of the samples at 750 °C in dry air results in a substantial increase of the catalytic activity. This is more pronounced in the NO conversion (Fig. 3c) and a low-temperature CO and hydrocarbon oxidation (Fig. 3a and b). The temperature of 50% NO conversion on bimetallic monoliths shifted by 100–130 °C to the low-temperature region after the thermal aging and was 245–257 °C. The temperatures of 50% CH and CO conversion also decreased by 30–40 °C after the aging (Fig. 3a and b) and were equal to 178–197 and 174–178 °C, respectively, on the aged samples with 0.17 g Pt/L–0.35 g Pd/L. However, the aging procedure led to a slight decrease in the efficiency of the high-temperature hydrocarbon oxidation over the bimetallic Pt–Pd–MnO_x–Al_2O_3 catalyst (at 400 °C, Fig. 4a), but its activity was still appreciably higher than that for the monometallic Pt–MnO_x–Al_2O_3 [10] and Pd–MnO_x–Al_2O_3 catalysts after thermal aging. The aging procedure had a similar influence on the ability of the bimetallic Pt–Pd–MnO_x–Al_2O_3 catalyst to remove NO (Fig. 4c). While after the thermal aging, the bimetallic Pt–Pd–MnO_x–Al_2O_3 catalyst provided CO conversion as high as 99.9% (Fig. 4b).

With increasing of Pd content in the bimetallic Pt–Pd–MnO_x–Al_2O_3 catalyst, the effect of the thermal aging on the hydrocarbon oxidative activity of the catalyst was found to decrease (Fig. 4a), and its influence on the ability to remove NO on the contrary amplifies (Fig. 4c). This fact indirectly proves that at temperatures 350–400 °C the selective catalytic reduction of NO by hydrocarbons takes place. The higher the hydrocarbon conversion in the oxidation reaction, the lower hydrocarbon consumption in the SCR of NO, as result the lower NO conversion achieved. This assumption is consistent with the results reported for catalyst Pd/Rh/Al_2O_3–CeO_2–ZrO_2 [31] and F-doped Pd/Al_2O_3 [32], but they were been tested at lower concentration of oxygen in the reaction mixture (2 vol.%).

Fig. 5 shows the effect of the duration of exposure to high temperatures (7 and 14 h) on the activity of two bimetallic Pt–Pd–MnO_x–Al_2O_3 catalysts with 0.17 g Pt/L–0.35 g Pd/L supported from platinum dinitrodiamine with palladium nitrate or with chloropalladic acid precursors (the MA-5PtNA-10PdN and MA-5PtNA-10PdClA catalysts, respectively). For both catalysts, the prolonged exposure to elevated temperature had no effect on their ability to oxidize CO, whereas their ability to reduce NO increased with increasing the duration of the thermal aging. The efficiency of hydrocarbons removal over these catalysts depended on the Pd precursors used. Thus, the catalytic activity of the ex-nitrate sample MA-5PtNA-10PdN in the oxidation of C_3H_8/C_3H_6 slightly decreased, while the ex-chloride catalyst MA-5PtNA-10PdClA continued to be activated. As a result, their activity in the hydrocarbons oxidation became close after the thermal aging at 750 °C for 14 h. The same three-way catalytic performance during the thermal aging was observed previously. The monometallic Pd and bimetallic PdPt and PdRh supported on ceria-promoted alumina retained or improved the efficiency of CO, C_3H_6 and NO removal after an aging under a cycled oxidizing-reducing environment at 900 °C [33] or in oxidative atmospheres at 1000–1100 °C [34]. Thermal aging of the 1.6 wt.% Pd/Al_2O_3 catalyst in flowing air at 700 °C improved its deNO*x* activity, while slightly diminished the CO and CH_4 oxidation activity [32]. On the other hand, thermal treatment under oxidizing aging atmospheres at 800 °C strongly affected the activity of

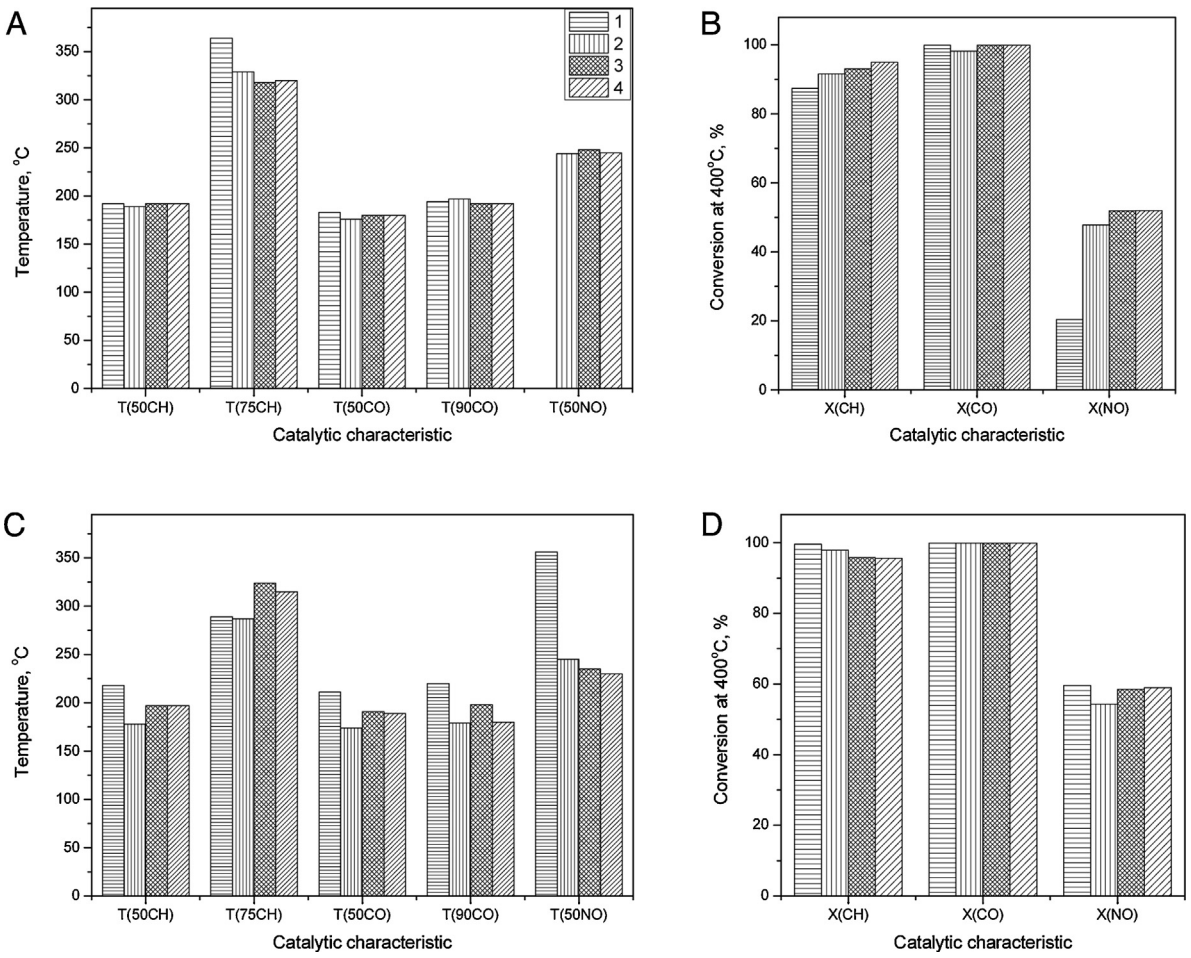

Fig. 5. Catalytic characteristics: Temperature of 50% and 75% conversion of propane/propene, T(50CH) and T(75CH); temperature of 50% and 90% conversion of carbon monoxide, T(50CO) and T(90CO); temperature of 50% conversion of nitrogen oxide, T(50NO); conversion of propane/propene, X(CH); conversion of CO, X(CO); conversion of NO, X(NO); at 400 °C over MA-5PtNA-10PdClA (A, B) and MA-5PtNA-10PdN (C, D) catalysts: fresh (1), aged at 750 °C in dry air for 7 h (2) and 14 h (3) and wet air for 7 h (4). Sample MA-5PtNA-10PdClA was prepared by using $Pt(NH_3)_2(NO_2)_2$ and H_2PdCl_4. Sample MA-5PtNA-10PdN was prepared by using $Pt(NH_3)_2(NO_2)_2$ and $Pd(NO_3)_2$.

the Pd–Rh/La–Ce–Al_2O_3 washcoated catalysts [35]; besides, their deactivation increased with time of the aging [35].

Fig. 5 presents also data on the effect of water vapor on the thermal aging of the bimetallic Pt–Pd–MnO_x–Al_2O_3 catalysts. One can see that the thermal aging in wet air at 750 °C did not decrease the catalytic performance of both studied catalysts; their catalytic characteristics in the removal of CO, hydrocarbons and NO are comparable with the properties of the samples aged in dry air. This result contradicts the generally accepted idea of rapid deactivation of TWC in the presence of water vapor [36,37].

The observed changes in the catalytic activity of the thermally aged bimetallic samples MA-5PtNA-10PdN and MA-5PtNA-10PdClA are likely to be associated with different sintering speeds of the noble metal particles. In this case, our results on the catalytic properties of the aged bimetallic Pt–Pd–MnO_x–Al_2O_3 catalysts are consistent with the well-known effects of structure insensitivity of CO oxidation over Pd/Al_2O_3 [38,39] and structure sensitive nature of NO reduction by CO [39], NO oxidation to NO_2 [25,28,40,41], and hydrocarbons oxidation over Pd/Al_2O_3 and Pt/Al_2O_3 [42–44]. There are the higher reaction activities over larger noble metal particles. The presence of chloride ions in the catalyst composition was shown to inhibit the reduction of noble metal oxides [43,45,46] and sintering of their particles [36,45,47–49] due to an anchoring as [PtClx] or [PdClx] complexes to the alumina surface [45,47]. On the other hand, platinum dinitrodiamine and palladium nitrate are not anchored on the alumina surface, and PtPd particles have weak interaction with alumina surface [46]. So, we can assume that the ex-nitrate catalyst MA-5PtNA-10PdN is more susceptible to sintering of the PtPd particles than the ex-chloride MA-5PtNA-10PdClA under the thermal aging, and therefore the former contains larger PtPd particles. On the other hand, the prolongation of the thermal aging leads to a decrease in the content of chloride ions in the aged ex-chloride catalyst; as a result, the catalytic properties can be improved. Chloride ions are supposed to inhibit the oxidation of hydrocarbons [45,50–52].

So, the bimetallic Pd–Pt–MnO_x–Al_2O_3 catalysts are characterized by high thermal stability both in dry and wet condition. Different studies on TWC and DOC have shown that the thermal aging is caused by a loss of surface area of the washcoating and sintering of active metal [32,33,37,53]. Below we will briefly discuss the textural and RedO*x* properties of the fresh and aged bimetallic Pd–Pt–MnO_x–Al_2O_3 catalysts, which allow their unique catalytic properties and thermal stability to be explained.

3.4. *A correlation between physico-chemical and catalytic properties of the fresh bimetallic Pt–Pd–MnO_x–Al_2O_3 monolith*

The doping of spinel-type structures of γ^*-Al_2O_3 by Mn^{3+} [4] and Mn_3O_4 by Al^{3+} cations [4,11,54,55] was discussed earlier and shown to result in a useful improvement of the catalytic performance of manganese-alumina catalysts in CO [10] and hydrocarbon (methane, *n*-C_4H_{10}, benzene and cumene) oxidation [4,11,54].

These spinel structures are formed at high temperature annealing (900–1000 °C) of γ-Al_2O_3 modified by manganese oxides (Table 1), so the effect was called thermoactivation [54,55]. The total Pt and Pd loading in MnO_x–Al_2O_3 washcoating layer was equal to or less than 0.75 wt.%, and it was not detectable by XRD.

HRTEM images with EDX spectra also show two spinel structures in the fresh Pd–Pt–MnO_x–Al_2O_3 catalyst, such as Mn^{3+}-γ^*-Al_2O_3 (Fig. 6A) and Al^{3+}-β-Mn_3O_4 (Fig. 6B), thus confirming the XRD data. The particles of the first spinel have a friable lamellar structure (Fig. 6A), which resembles the crystal structure reported for γ-Al_2O_3 [56]. Their interplanar spacing of 0.448 nm was close to the (1 1 1) plane of γ-Al_2O_3 [56]. According to EDX, these γ-Al_2O_3 particles are doped with Mn^{n+} cation in the amount of 12–22 at.%. The second image clearly shows the well-crystallized (2 1 1) lattice plane with a d-spacing of 0.249 nm, which confirms the tetragonal phase of the β-Mn_3O_4 crystal structure [57]. Some HRTEM images of the particles enriched with Mn^{n+} are characterized by interplanar spacings of 0.276 and 0.313 nm, which are coincident with those of (1 0 3) and (1 1 2) planes of tetragonal Mn_3O_4 [57]. The Mn_3O_4 nanoparticles exhibit a thin isolated platelet-like morphology. As indicated by EDX, the content of Al^{3+} doped Mn_3O_4 varied within 26–28 at.%.

Pt and Pd are likely to be contained in the fresh Pd–Pt–MnO_x–Al_2O_3 monolith as clusters and identified by dotted contrast variation in the HRTEM images (marked with arrows on Figs. 6 and 7). A comparison of TEM images of the ex-chloride MA-5PtNA-10PdClA (Fig. 6) and ex-nitrate MA-5PtNA-10PdN (Fig. 7) samples showed that the Pd precursors had a very slight effect on the size of the Pt and Pd clusters contained in the fresh catalyst, though for the ex-chloride-free sample the weak tendency to slightly larger size of particles is traced.

Fig. 8 shows the curves of temperature programmed reduction with hydrogen of the fresh bimetallic Pd–Pt–MnO_x–Al_2O_3 monoliths. The fresh catalyst MA-5PtNA-10PdClA prepared by using platinum dinitrodiamine and chloropalladic acid is characterized by the broad peak of hydrogen uptake with a maximum at 175 °C (Fig. 8A, curve 1). The amount of absorbed hydrogen exceeds by a factor of 2.78 the hydrogen amount required for the reduction of PdO and PtO_2 to metal. However, the amount of hydrogen absorbed by MA-5PtNA-10PdClA corresponds well to the reduction of Mn^{3+} cations to Mn^{2+}, assuming that ca. 80–85% of them enter the composition of Mn_3O_4. This suggests that the reduction of noble metal oxides is accompanied by the reduction of γ^*-Al_2O_3-doped Mn^{3+} cations and Mn_3O_4. The fresh ex-nitrate sample MA-5PtNA-10PdN is reduced in a similar manner; however, it has a somewhat higher rate of hydrogen uptake in the temperature regions of 80–100 and 230–300 °C (Fig. 8B, curve 1).

Of particular interest are three features of the reduction behavior of the Pd–Pt–MnO_x–Al_2O_3 catalyst. First, manganese(III) cations in this catalyst are reduced at lower temperatures as compared to the bulk [58] and Al_2O_3-supported [5,9,59] Mn_2O_3 and Mn_3O_4 oxides. It is known that Mn_2O_3 supported on alumina and calcined at 800 °C is reduced by hydrogen in a stepwise manner: first to Mn_3O_4 at 330 °C and then to MnO at 425 °C [5]. A strong interaction between manganese oxide and alumina having a high specific surface area often hinders the reduction of MnO_x, which is characterized in TPR experiments by unresolved low-intensity peaks in the temperature region of 200–650 °C [60]. As shown in our earlier study [9] of the manganese-alumina system calcined at 900 °C, the easily (170–270 °C) and difficultly (310–480 °C) reducible compounds correspond to Mn_3O_4 spinel doped with Al^{3+} cations and $(Mn,Al)[Al]_2O_4$ spinel containing Mn^{3+} cations, respectively. Mn^{3+} cation in them reduced to Mn^{2+} and was characterized by a H_2/Mn ratio with a greater stoichiometric value for the reduction of Mn_3O_4 (0.42–0.44 instead of 0.33).

Second, the presence of manganese oxide, in its turn, facilitates the reduction of Pt oxide in Pd–Pt–MnO_x–Al_2O_3 catalysts (Fig. 8) as compared to the catalyst not containing manganese cations. For example, the Cl-containing PtO_2 particles in Pt/Al_2O_3 are reduced at 220–290 and 380 °C [61], the difference in reducibility of oxychlorinated species being related to a transition from the bulk particles to the two-dimensional particles strongly interacting with alumina [61,62]. The chloride-free PtO*x* particles are reduced in the same temperature range [63]. Strengthening of the interaction between highly dispersed PtO*x* particles and Al_2O_3 deteriorates their reducibility, thus shifting the hydrogen absorption peaks to 420–440 °C [64]. At low temperatures, reducibility by hydrogen is incident only to the highly dispersed surface particles PtO and α-PtO_2, which are formed in the oxidation of metallic Pt particles at 25–100 °C [62] and 200–400 °C [43,61,62,65], respectively. The surface PtO and α-PtO_2 particles are reduced at a temperature not higher than 50 °C [62] and near 100 °C [47,61,62], respectively.

Third, it is known that alumina-supported PdO*x* particles have a higher reducibility by hydrogen in comparison with PtO*x*, but the temperature range of their reduction strongly depends on PdO morphology and strength of the interaction with the support. The easily reducible PdO*x* species reduce yet at room temperature [65]. The PdO—particles reducible between 50 and 130 °C are considered to be relatively stable [32]. The two-dimensional surface PdO*x* complexes characterized by the broad peak of hydrogen uptake at 300–350 °C are attributed to the stable species that are strongly interacting with the support [9,32]. As in the case of PtO*x*, the reduction of surface PdO particles, which are easily generated upon oxidation of large metal particles to a depth of several monolayers [66], starts at room temperature [46]. Thus, it can be supposed that Mn^{3+} cations and PtOx clusters hinder the formation of relatively stable PdO particles in the bimetallic catalysts Pd–Pt–MnO_x–Al_2O_3 as compared to Pd/Al_2O_3. The PdO particles, which prevail in the former catalysts and strongly interact with the support, are reduced more easily than in Pd/Al_2O_3 catalysts; this may be related to the formation of mixed PdO*x*-PtO_x clusters.

Thus, the fresh bimetallic Pd–Pt–MnO_x–Al_2O_3 monoliths contain the particles of PtO*x*, PdO and Mn^{3+} cation, which determine the RedO*x* properties of the catalyst and are reduced in the same temperature range. Taking into account their temperature range of reduction (between 100 and 250 °C), it can be supposed that PtO*x* and PdO are quite stable and strongly interact with components of the support. An improvement of the reduction behavior of manganese oxide and noble metal oxides in Pd–Pt–MnO_x–Al_2O_3 is commonly attributed to hydrogen spillover from a noble metal to MnO*x* [5,67] and to an increased mobility of the lattice oxygen in the oxides [5,46], which is possible only in the case of close contact between MnO*x* particles and noble metal oxides.

The catalytic effect of noble metal on the reduction of manganese oxide is consistent with the positive effect of Pt and Pd on the activity of MnO_x–Al_2O_3 catalyst for the oxidation of butane (Table 2, samples N 2–6 and 7–11 compared with sample no. 1), propane/propene mixture and CO as well as the reduction of NO (Table 4, sample N 2–4 compared to N 1). The non-additive increase in the catalytic activity of the bimetallic catalyst Pd–Pt–MnO_x–Al_2O_3 compared with monometallic catalysts (Tables 2 and 3) is suggested to connect with a formation of PdO–PtO_x clusters on the surface of Mn_3O_4 and a modification of alumina structure by Mn^{3+} and PtPd clusters. The former improves the RedO*x* properties of the catalysts.

According to TPR and HRTEM study, the reduction properties and morphology of the particles of fresh catalysts synthesized from palladium nitrate and chloropalladic acid are virtually identical and hence independent of the features of a Pd precursor. In this case, the difference in catalytic characteristics of the fresh bimetallic Pd–Pt–MnO_x–Al_2O_3 monoliths obtained from different Pd precur-

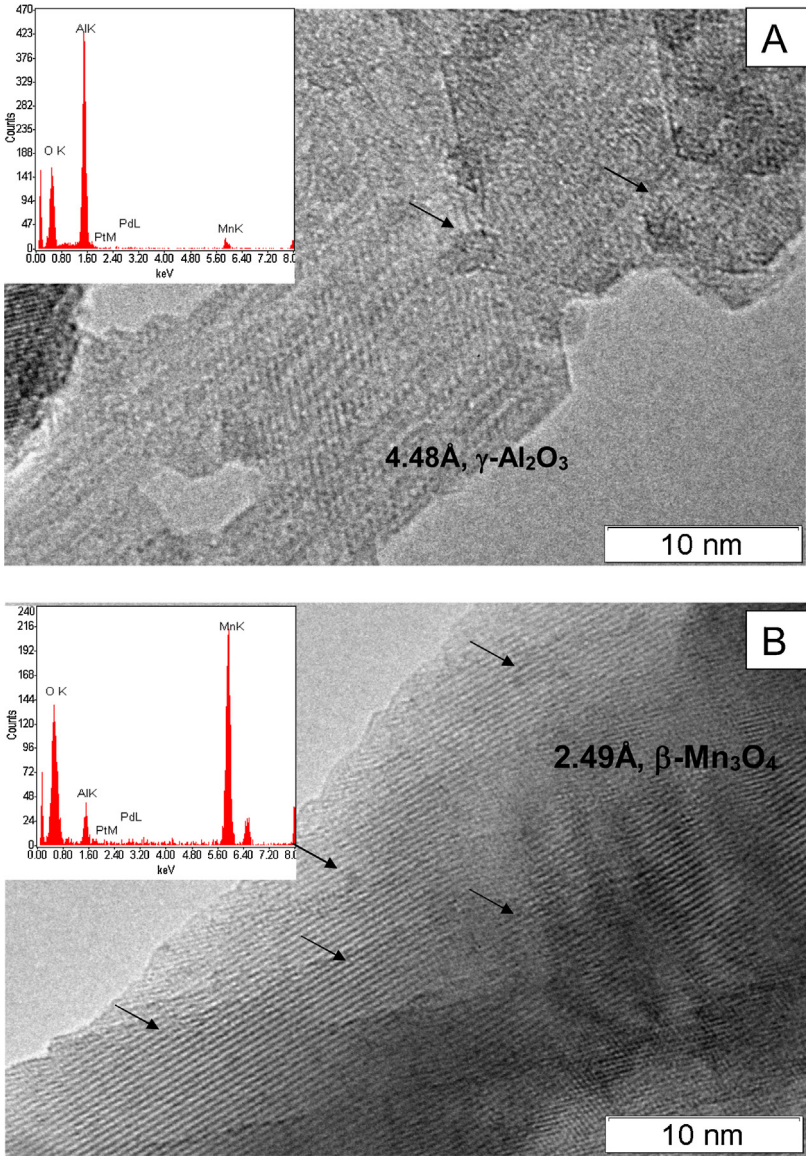

Fig. 6. HRTEM images and EDX spectra of alumina particles doped with Mn^{3+} cation (A) and manganese oxide particles doped with Al^{3+} cation (B) observed in fresh MA-5PtNA-10PdClA catalyst. The arrows indicate noble metal particles.

sors can be attributed only to the inhibiting action of chloride ions on the oxidation of hydrocarbons and CO as well as on the reduction of NO.

3.5. *A correlation between physico-chemical and catalytic properties of the aged bimetallic Pt–Pd–MnO_x–Al_2O_3 monolith*

Table 1 gives the XRD composition and textural characteristics of the washcoating layer aged in a flow of dry or wet air at 750 °C. The data of Table 1 show no changes in the phase composition of washcoating layer of the Pd–Pt–MnO_x–Al_2O_3 monolith during aging. The washcoating layer contains a mixture of two spinels, Mn^{3+}-γ*-Al_2O_3 (*a*—7.94–7.95 Å) and Al^{3+}-β-Mn_3O_4 (*a*—8.05–8.15 Å). The Pt and Pd phases were not detectable by XRD due to their low loading in the MnO_x–Al_2O_3 washcoating layer. Slight changes in the textural characteristics peculiar to the aged washcoating layer of the Pd–Pt–MnO_x–Al_2O_3 catalyst are in the range of measurement error. It is likely due to the high-temperature calcination (900 °C for 4 h) of the fresh MnO_x–Al_2O_3 washcoating layer. TEM images presented on Figs. 9 and 10 clearly illustrate that the noble metal particles sintered under the thermal aging, in contrast to the particles of MnO_x–Al_2O_3 washcoating that showed no changes in the phase composition and textural properties. Besides, the noble metal particles sintered more slowly in the MA-5PtNA-10PdClA sample prepared by using chloropalladic acid as compared with the ex-nitrate MA-5PtNA-10PdN monolith. For the aged MA-5PtNA-10PdClA sample, HRTEM images show two types of PtPd particles located on alumina and differing in the size and morphology. Particles of the first type (Fig. 9A) are located over alumina particles doped with manganese cations, have a spherical shape and are 2–3 nm in size with d-spacing of 0.204–0.208 nm. They contain mainly Pd, with atomic ratio Pt/Pd near 15/85. The other particles (Fig. 9B) have a flat shape without smooth boundary, which may indicate their strong interaction with washcoating material enriched with Mn^{n+}. They are 10–15 nm in size and are characterized by interplanar spacing of 0.221 nm, which is close to the (1 1 1) plane of metallic Pt, Pd or PtPd-alloy crystal structure. The composition of most metallic particles is quite heterogeneous and atomic Pt/Pd ratio in them varied from 20/80 to 40/60 by EDX analysis.

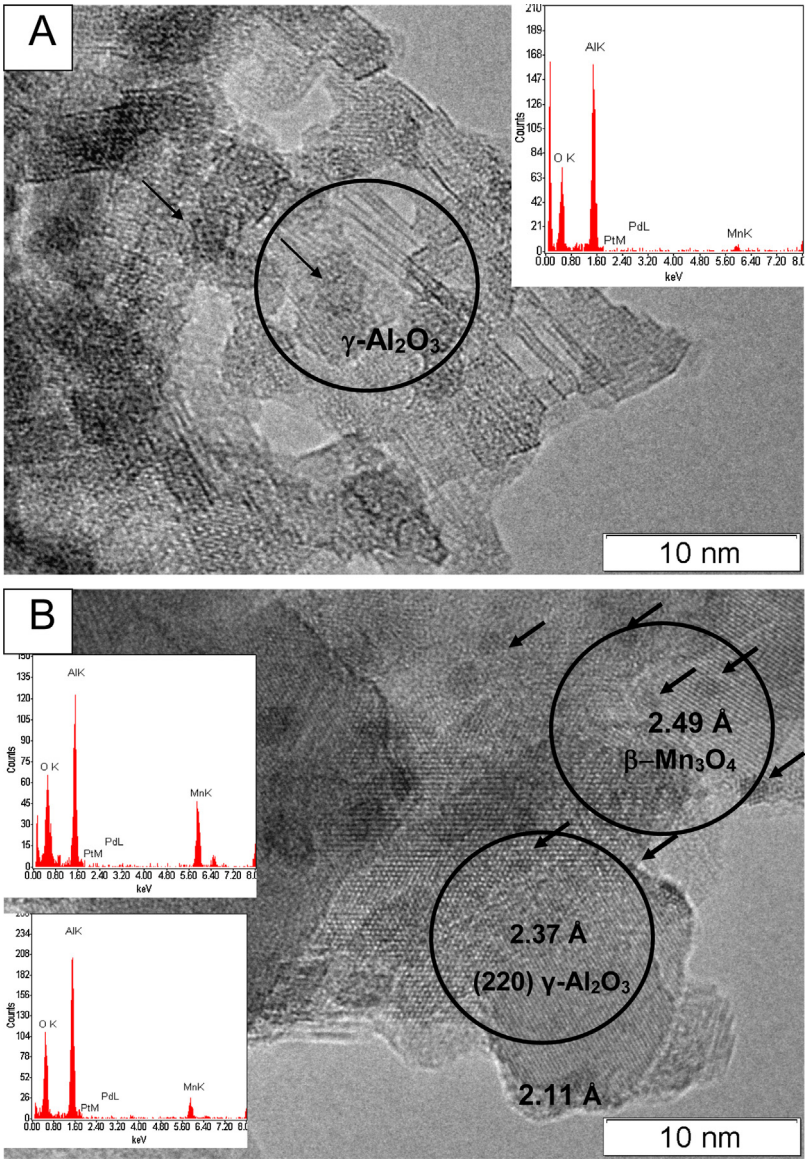

Fig. 7. HRTEM images and EDX-spectra of alumina particles doped by Mn^{3+} cation (A) and manganese oxide particles doped by Al^{3+} cation (B) observed in fresh MA-5PtNA-10PdN catalyst. The arrows indicate noble metal particles.

The aged ex-nitrate MA-5PtNA-10PdN sample was detected by HRTEM to contain three types of noble metal particles. The first type particles (Fig. 10A) in the form of hemispheres have a size of 20–25 nm and d-spacing equal to 0.228–0.229 nm. The observed interplanar spacing indicates that the composition of the Pt-Pd particles corresponds to metallic state. According to EDX analysis, they are enriched with Pd, the atomic ratio of Pt/Pd in them is rather homogeneous and equal to 30/70–37/63. They have probably a weak interaction with γ^*-Al_2O_3 doped with manganese cations. Particles of the second type (Fig. 10B) do not have a specific shape. They have a size of 20–30 nm with d-spacing of 0.228 nm. The composition of most particles is quite homogeneous with a prevalence of platinum, atomic ratio of Pt/Pd was 70/30. They are located on the areas with high concentrations of manganese cations and apparently have a strong interaction with the washcoating material. Particles of the third type (Fig. 10C) are located on border of coalescence of alumina particles doped with manganese cations, have a spherical shape and are near 5 nm in size. Their d-spacing of 0.194–0.195 nm correspond to the (2 0 0) plane of metal Pt, Pd or PtPd-alloy.

Changes in the structure of PtPd particles caused by the thermal aging of the PdPt–MnO_x/Al_2O_3 samples were confirmed experimentally by TPR-H_2. Fig. 8 shows the curves of temperature programmed reduction with hydrogen of the bimetallic Pd–Pt–MnO_x–Al_2O_3 monoliths aged under different conditions. After thermal aging in dry and wet air, the reduction profiles of the bimetallic Pd–Pt–MnO_x–Al_2O_3 samples have changed.

In addition to the main peak with a maximum at 175 °C, the spectrum of the MA-5PtNA-10PdClA sample aged in dry air has two low-temperature peaks with the maxima at 40 and 70 °C (Fig. 8A, curve 2). According to data reported in [46,47,61,62,66], these peaks indicate the presence of highly dispersed surface oxides PtO and/or PdO that are formed via the oxidation of metal particles during pretreatment of the sample before the TPR experiment. The size of metal particles formed under thermal aging in dry air is evidently small because they are completely oxidized during the pretreatment in oxygen at 500 °C for 0.5 h. These particles reside most likely on the alumina surface since the presence of peaks at 40 and 70 °C does not affect the position and intensity of the main peak of hydrogen uptake at 175 °C and hence produces no effect on the reduction

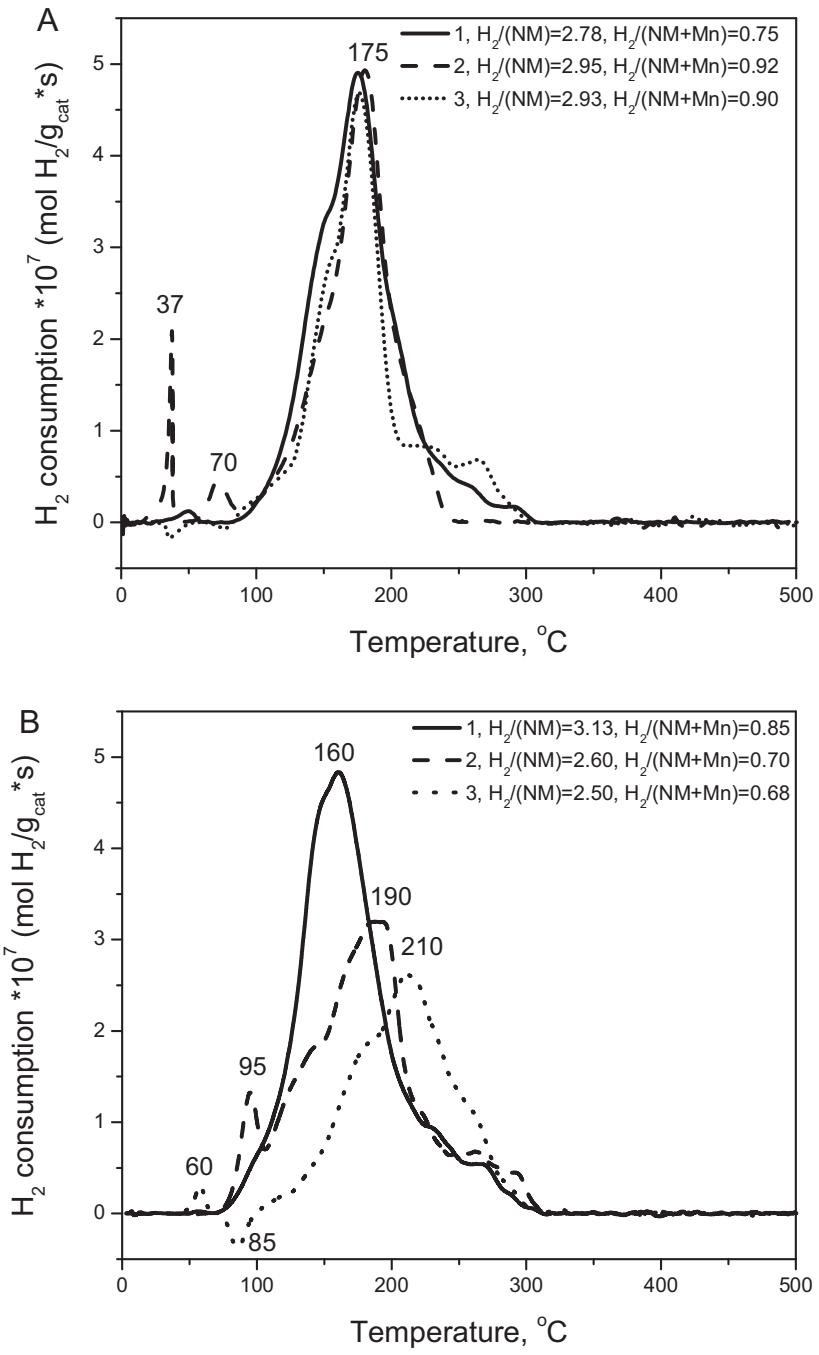

Fig. 8. H_2-TPR curves of MA-5PtNA-10PdClA (A) and MA-5PtNA-10PdN (B) catalysts fresh (1), aged at 750 °C in dry air (2) and wet air (3). Sample MA-5PtNA-10PdClA was prepared by using $Pt(NH_3)_2(NO_2)_2$ and H_2PdCl_4. Sample MA-5PtNA-10PdN was prepared by using $Pt(NH_3)_2(NO_2)_2$ and $Pd(NO_3)_2$. Molar ratio of H_2 consumed during TPR to theoretical H_2 amount required for reduction of PtO_2 and PdO to metal (H_2/NM) and to theoretical H_2 amount required for reduction of PtO_2 and PdO to metal and Mn_3O_4 to MnO H_2/(NM + Mn).

rate of the major part of PtO_2/PdO and Mn_3O_4 particles closely contacting each other. The fraction of small surface PtO/PdO particles does not exceed 15% of the total Pt–Pd content in the MA-5PtNA-10PdClA catalyst; according to TEM with EXD analysis, they are enriched with palladium and have a size of 2–3 nm (Fig. 9A). The metal PtPd particles, which are 10–15 nm in size according to TEM and located on the support crystallites enriched with Mn^{3+} (Fig. 9B), are easily oxidized upon pretreatment before the TPR experiment and do not change their reduction potential with respect to the fresh catalyst.

The TPR profile of the MA-5PtNA-10PdClA catalyst aged in wet air (Fig. 8A, curve 3) has the peak of hydrogen release at a temperature of 40–70 °C. This peak corresponds to decomposition of palladium hydride [46,65] and indicates the presence of a minor amount of metallic Pd in the sample. The Pd particles are highly stable because they are not oxidized during pretreatment in oxygen before the TPR experiment. However, a large part of PtO_2/PdO and Mn_3O_4 particles, which are in close contact with each other, do not change their size and oxidation state in comparison with the sample aged in dry air (Fig. 8A, curve 2).

Aging in dry air produces stronger changes in reducibility of the MA-5PtNA-10PdN catalyst (Fig. 8B, curve 2) as compared to MA-5PtNA-10PdClA. After thermal aging, the reduction profile of the sample contains a well-defined peak at 95 °C, the main peak is

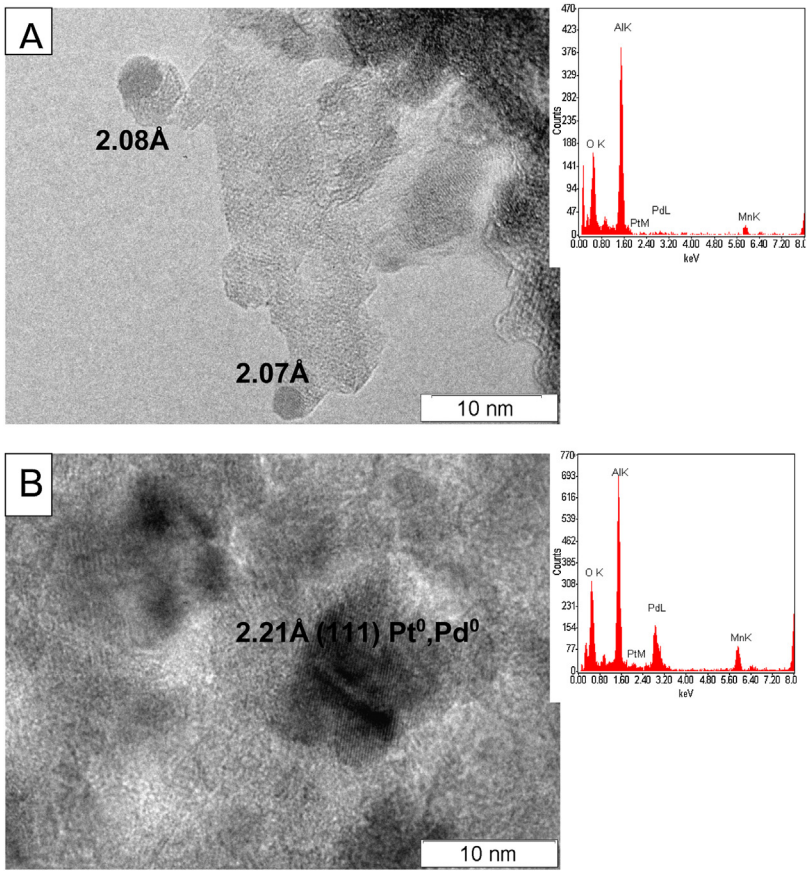

Fig. 9. HRTEM images and EDX spectra of small (A) and large (B) PtPd particles located on alumina particles doped with Mn^{3+} cation in MA-5PtNA-10PdClA aged in dry air at 750 °C for 14 h.

shifted to higher temperatures from 175 to 190 °C, and the latter is less intensive than for the fresh sample (Fig. 8B, curve 2). The first peak on the TPR-H_2 curves and the TEM data testify to the presence of metal PtPd particles in the aged MA-5PtNA-10PdN sample (Fig. 10A); upon treatment of the sample in oxygen, the surface of such particles is oxidized to the highly dispersed α-PtO_2/PdO particles. A high-temperature shift of the main peak may indicate a stronger interaction of the PtO_2/PdO particles, which are formed by the oxidation of 20–30 nm metal particles (Fig. 10B), with components of the support in comparison with the fresh catalyst. The observed decrease in the amount of hydrogen absorbed by the aged MA-5PtNA-10PdN samples can be attributed both to the presence of the Pt–Pd alloy particles, which are not oxidized under treatment in oxygen, and to the decrease in the amount of Mn_3O_4 and Mn^{3+}-doped alumina. However, XRD did not show the formation of new phases—MnO and stoichiometric spinel $MnAl_2O_4$ as well as the crystallized particles of Pt–Pd alloy.

After aging in wet air, the TPR spectrum of the MA-5PtNA-10PdN catalyst has the peaks of hydrogen absorption and release, which appear at 60 and 85 °C, respectively (Fig. 8B, curve 3). Close areas of the peaks clearly show that they correspond to the formation of palladium hydride from metal Pd particles and its decomposition. Aging of the MA-5PtNA-10PdN sample in wet air increases the high-temperature shift of the main peak of hydrogen uptake from 190 to 210 °C, which indicates a decrease in the reduction potential of the catalyst.

A comparison of TPR and TEM data for the aged samples MA-5PtNA-10PdClA and MA-5PtNA-10PdN allows a conclusion that in the latter case the noble metal particles are more prone to sintering during the thermal aging in both the dry and wet air. Therewith, the formation of larger noble metal particles improves the DeNOx behavior and activity in the oxidation of hydrocarbons for both aged bimetallic Pd–Pt–MnO_x–Al_2O_3 catalysts. This is due to structure sensitivity of the indicated reactions over Pd-containing catalysts [39,42,43,44], which produces size effects in the catalytic behavior. The observed decrease in the temperature of 50% NO conversion over the aged catalyst in comparison with the fresh one is related to differences in the mechanism of NO reduction. Supposedly, NO reduction on the aged catalyst proceeds in the region of lower temperatures because the reduction involves carbon monoxide. It is known that high activity of Pd-containing catalysts in NO reduction by carbon monoxide is observed at 245–270 °C [31,32,37]. However, on the fresh catalyst NO is reduced by propane/propene, so the maximum DeNO*x* activity of Pd-containing catalysts is observed at temperatures above 300 °C [31,32]. The route of NO reduction by propane/propene is switched to the structure sensitive reduction by carbon monoxide due to the formation of larger PtPd particles upon aging. In the temperature region of 400 °C, nitric oxide is reduced by propane/propene on both the fresh and aged catalyst; so, no changes are observed in the NO conversion at 400 °C after aging of the MA-5PtNA-10PdN and MA-5PtNA-10PdNN catalysts synthesized from chloride-free Pt–Pd compounds. The improvement of high-temperature performance of the MA-5PtNA-10PdClA catalyst synthesized with chloropalladic acid is caused by both the coarsening of PtPd particles and the removal of chloride ions from the catalyst surface under thermal aging.

The catalytic activity in hydrocarbon oxidation was earlier shown to correlate with both the PtPd particles size [43,44] and the PdO–Pd phase transformation [31]. Thus, the formation of nanoscale PdO–PtO_x particles from their clusters on the surface of

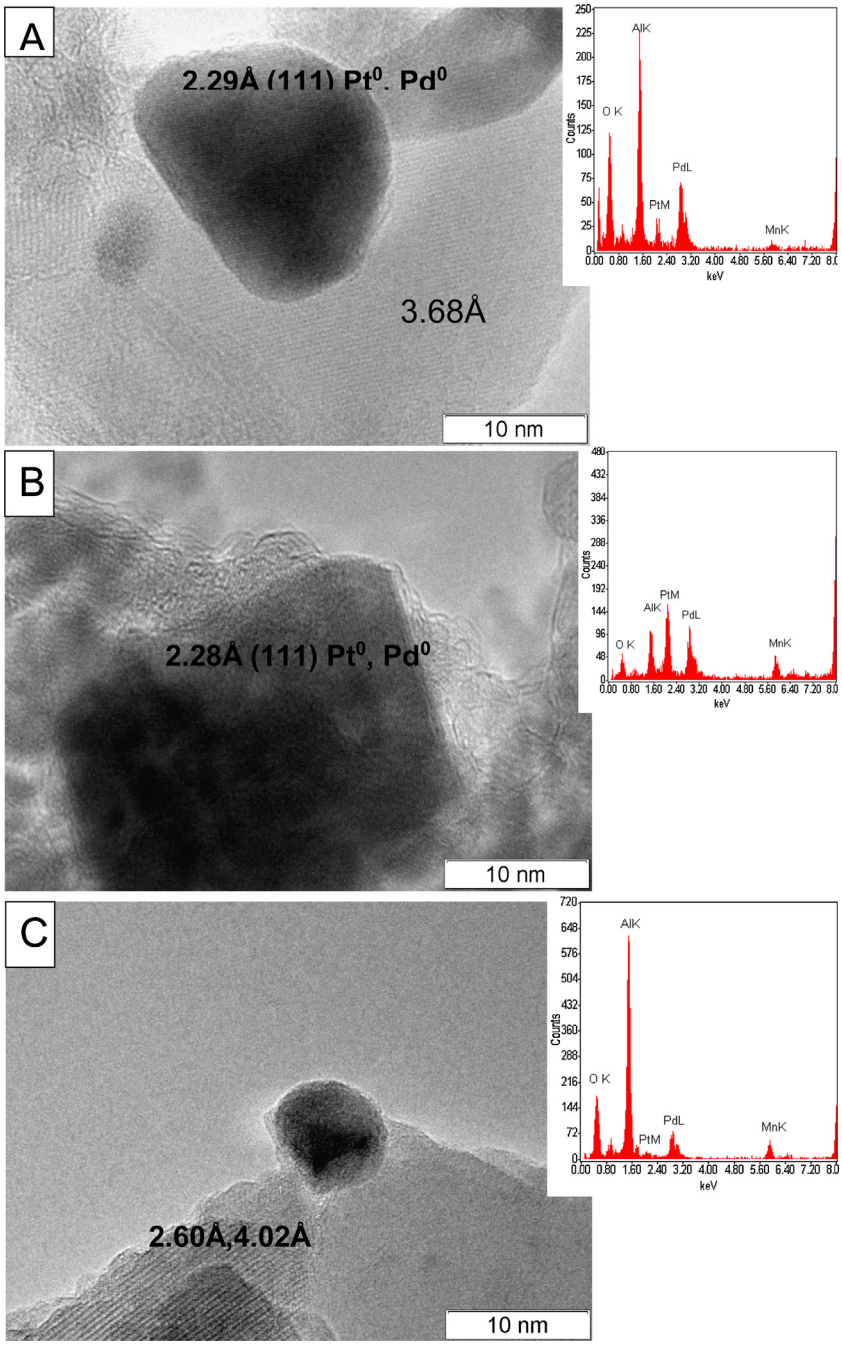

Fig. 10. HRTEM-images and EDX-spectra of three type of large (A,B) and small (C) metallic PtPd particles located on alumina particles doped by Mn^{3+} cation in MA-5PtNA-10PdN aged in dry air at 750 °C for 14 h.

Mn_3O_4 produces an observable improvement of the light-off properties of the aged Pt–Pd–MnO_x–Al_2O_3 catalysts in the oxidation of propane/propene mixture (Fig. 3). On the contrary, the phase transition PdO–PtO_x → Pd(Pt) decreases the achievable conversion of hydrocarbons at 400 °C in the DIESEL test (Fig. 4). This assumption correlates well with the known higher activity of PdO in the oxidation of propane [31,68] and methane [42,43,51,69] as compared to metallic palladium, and with stabilization of metallic state of palladium in the presence of propane already at 350 °C even in the oxygen-containing mixtures [31,68].

A weak effect of thermal aging on catalytic performance of the Pt–Pd–MnO_x–Al_2O_3 monolith in the oxidation of carbon monoxide is related to insensitivity of this reaction to both the size of noble metal particles [38,39] and the valent state of Pd [31,70].

4. Conclusions

The present study was devoted to the development of a monolithic catalyst with a low content of noble metals for purification of diesel engine exhaust.

The catalytic activity of the optimal Pt–Pd–MnO_x–Al_2O_3 monolithic catalysts in butane oxidation and in the DIESEL test experiments has been found to depend on the Pt and Pd precursor, total noble metal loading and atomic Pt/Pd ratio. At a similar Pt loading (0.17 g/L) and precursor, the catalytic activity in oxidation reaction increases in the order: $H_2PdCl_4 \sim Pd(NH_3)_4(NO_3)_2 < Pd(NO_3)_2 \sim Pd(CH_3COO)_2$. When one Pd precursor is used, the catalytic performance in CO and hydrocarbon oxidation improves with the Pd loading increase from 0 to

0.35 g/L, and is nearly constant at a higher Pd loading (0.70 g/L). The catalytic activity also increases with atomic Pt/Pd ratio.

Advantages of the synergetic effects of Pt, Pd and manganese oxides observed in the reactions of hydrocarbon oxidation resulted in the development of a new diesel exhaust catalyst with a Pt loading as low as 0.17 g/L instead of the traditional amount of 0.70 g/L at the Pd loading of 0.35 g/L. The Pt–Pd–MnO_x–Al_2O_3 catalyst has high activity in low temperature oxidation of light hydrocarbons, and high thermal stability. At 400 °C the CH, CO and NO conversions on the aged catalysts with 0.17 g Pt/L and 0.35 g Pd/L loading are 97.5, 99.9 and 56%, respectively. The temperatures of 50% conversion of CH, CO and NO are 183, 176 and 251 °C, respectively. These characteristics are superior to those typical of Pt–MnO_x–Al_2O_3 and Pd–MnO_x–Al_2O_3 catalysts containing 0.70 g/L of Pt or Pd.

The catalytic activity in light hydrocarbon oxidation is shown to correlate with the RedO*x* properties of PdPt–MnO_x–Al_2O_3 catalysts and Pt–Pd particle size. The non-additive increase in the catalytic activity of the bimetallic catalyst is suggested to connect with a formation of PdO–PtO_x clusters on the surface of Mn_3O_4 and a modification of alumina structure by Mn^{3+} and PtPd clusters. The improvement of catalytic performance of the aged catalysts in the reactions of hydrocarbon oxidation and NO reduction can be related to coarsening of the clusters to nanoscale PdO–PtO_x particles, which are characterized by the reversible RedO*x* transformations of Pd(Pt)–PdO(PtO_x)–Pd(Pt) during TPR and catalytic experiments.

Acknowledgement

This work was supported by the Federal Agency of Scientific Organizations (V46.5.6). The authors are very obliged Ishchenko A.V. for HRTEM investigation.

References

[1] R.M. Heck, R.J. Farrauto, Catalytic Air Pollution Control, Commercial Technology, New York, VNR, 1995, pp. 206.
[2] M.V. Twigg, Catal. Today 117 (2006) 407–418.
[3] H.S. Gandhi, G.W. Graham, R.W. McCabe, J. Catal. 216 (2003) 433–443.
[4] V.V. Yashnik, Z.R. Kuznetsov, V.A. Ismagilov, N.M. Ushakov, Top. Catal. 30–31 (2004) 293–298.
[5] J. Carno, M. Ferrandon, E. Bjornbom, S. Jaras, Appl. Catal. A: Gen. 155 (1997) 265–281.
[6] M. Ferrandon, J. Carno, S. Jaras, E. Bjornbom, Appl. Catal. A: Gen. 180 (1999) 141–151.
[7] Y.J. Mergler, J. Hoebink, B.E. Nieuwenhuys, J. Catal. 167 (1997) 305–313.
[8] B.E. Nieuwenhuys, Adv. Catal. 44 (1999) 259–328.
[9] S.A. Yashnik, Z.R. Ismagilov, V.V. Kuznetsov, V.A. Ushakov, V.A. Rogov, I.A. Ovsyannikova, Catal. Today 117 (2006) 525–535.
[10] S.A. Yashnik, Z.R. Ismagilov, A.V. Porsin, S.P. Denisov, N.M. Danchenko, Top. Catal. 42-43 (2007) 465–469.
[11] Z.R. Ismagilov, N.V. Shikina, S.A. Yashnik, A.N. Zagoruiko, M.A. Kerzhentsev, V.A. Ushakov, V.A. Sazonov, V.N. Parmon, V.M. Zakharov, B.I. Braynin, O.N. Favorskii, Catal. Today 155 (2010) 35–44.
[12] F. Diehl, J. Barbier Jr., I. Duprez, G. Guibard, Appl. Catal. B: Environ. 95 (2010) 217–227.
[13] G. Mabilon, D. Durand, Ph. Courty, Stud. Surf. Sci. Catal. 96 (1995) 775–788.
[14] M.H. Wiebenga, C.H. Kim, S.J. Schmieg, S.H. Oh, D.B. Brown, D.H. Kim, J.-H. Lee, C.H.F. Peden, Catal.Today 184 (2012) 197–204.
[15] A. Morlang, U. Neuhausen, K.V. Klementiev, F.-W. Schutze, G. Miehe, H. Fuess, E.S. Lox, Appl. Catal. B: Environ. 60 (2005) 191–199.
[16] J. Andersson, M. Antonsson, L. Eurenius, E. Olsson, M. Skoglundh, Appl. Catal. B: Environ. 72 (2007) 71–81.
[17] L. Olsson, M. Abul-Milh, H. Karlsson, E. Jobson, P. Thormahlen, A. Hinz, Top. Catal. 30–31 (2004) 85–90.
[18] H. Oh, J. Luo, W.S. Epling, Catal. Lett. 141 (2011) 1746–1751.
[19] M. Al-Harbi, R. Hayes, M. Votsmeier, W.S. Epling, Can. J. Chem. Eng. 90 (2012) 1527–1538.
[20] R. Burch, P.J. Millington, Catal. Today 26 (1995) 185–206.
[21] W. Xiaodong, Y. Haining, W. Duan, L. Shuang, F. Jun, J. Rare Earths 31 (2013) 1141–1147.
[22] G. Qi, W. Li, Catal. Today 258 (2015) 205–213.
[23] K. Irani, W.S. Epling, R. Blint, Appl. Catal. B: Environ. 92 (2009) 422–428.
[24] P. Bourges, G. Lunati, S. Mabilon, Stud. Sur. Sci. Catal. 116 (1998) 213–222.
[25] A. Boubnov, S. Dahl, E. Johnson, A.P. Molina, S.B. Simonsen, F.M. Cano, S. Helveg, L.J. Lemus-Yegres, J.-D. Grunwaldt, Appl. Catal. B: Environ. 126 (2012) 315–325.
[26] A. Setiabudi, M. Makkee, J.A. Moulijn, Appl. Catal. B: Environ. 50 (2004) 185–194.
[27] W.S. Epling, L.E. Campbell, A. Yezerets, N.W. Currier, J.E. Parks, Catal. Rev. 46 (2004) 163–245.
[28] E. Olsson, L. Fridell, J. Catal. 210 (2002) 340–353.
[29] M. Koebel, M. Elsener, G. Madia, SAE Tech. Pap. Ser. 2001 (2001) 01–3625.
[30] C.S. Sluder, J.M. Storey, S.A. Lewis, L.A. Lewis, SAE Tech. Pap. Ser. 2005 (2005) 01–1858.
[31] L. Martın, J.L. Arranz, O. Prieto, R. Trujillano, M.J. Holgado, M.A. Galan, V. Rives, Appl. Catal. B: Environ. 44 (2003) 41–52.
[32] S.K. Matam, E.H. Otal, M.H. Aguirre, A. Winkler, A. Ulrich, D. Rentsch, A. Weidenkaff, D. Ferri, Catal. Today 184 (2012) 237–244.
[33] J.R. Gonzalez-Velasco, J.A. Botas, R. Ferret, M.P. Gonzalez-Marcos, J.-L. Marc, M.A. Gutierrez-Ortiz, Catal. Today 59 (2000) 395–402.
[34] H. Shinjoh, H. Muraki, Y. Fujitani, Stud. Surf. Sci. Catal. 71 (1991) 617–628.
[35] J. Barbier Jr., D. Duprez, Appl. Catal. B: Environ. 4 (1994) 105–140.
[36] T. Tabata, K. Baba, H. Kawashima, Appl. Catal. B: Environ. 7 (1995) 19–32.
[37] M. Boudart, Chem. Rev. 95 (1995) 661–666.
[38] D.R. Rainer, M. Koranne, S.M. Vesecky, D.W. Goodman, J. Phys. Chem. B 101 (1997) 10769–10774.
[39] R.F. Hicks, H. Qi, M.L. Young, R.G. Lee, J. Catal. 122 (1990) 280–294.
[40] E. Xue, K. Seshan, J.R.H. Ross, Appl. Catal. B 11 (1996) 65–79.
[41] S.S. Mulla, N. Chen, L. Cumaranatunge, G.E. Blau, D.Y. Zemlyanov, W.N. Delgass, W.S. Epling, F.H. Ribeiro, J. Catal. 241 (2006) 389–399.
[42] S.K. Matam, M.H. Aguirre, A. Weidenkaff, D. Ferri, J. Phys. Chem. C 114 (2010) 9439–9443.
[43] R.F. Hicks, H. Qi, M.L. Young, R.G. Lee, J. Catal. 122 (1990) 280–294.
[44] Y.-F.Y. Yao, J. Catal. 87 (1984) 152–162.
[45] D. Simone, T. Kennelly, N.L. Brungard, R.J. Farrauto, Appl Catal 70 (1991) 87–100.
[46] S.A. Yashnik, Z.R. Ismagilov, Top. Catal. 55 (2012) 818–836.
[47] H. Lieske, G. Lietz, H. Spindler, W. Hanke, J. Volter, J. Catal. 81 (1983) 17–25.
[48] D.D. Beck, C.J. Carr, J. Catal. 110 (1988) 285–297.
[49] Z.R. Ismagilov, S.A. Yashnik, A.N. Startsev, A.I. Boronin, A.I. Stadnichenko, V.V. Kriventsov, S. Kasztelan, D. Guillaume, M. Makkee, J.A. Moulijn, Catal. Today 144 (2009) 235–250.
[50] T.R. Baldwin, R. Burch, Appl. Catal. 66 (1990) 359–381.
[51] R.J. Farrauto, M.C. Hobson, T. Kennelly, E.M. Waterman, Appl. Catal. A Gen. 81 (1992) 227–237.
[52] M.L. Toebes, J.A. van Dillen, K.P. de Jong, J. Mol. Catal. A Chem. 173 (2001) 75–98.
[53] I. Heo, J.W. Choung, P.S. Kim, I.-S. Nam, Y. Song, C.B. In, G.K. Yeo, Appl. Catal. B: Environ. 92 (2009) 114–125.
[54] P.G. Tsyrulnikov, V.S. Salnikov, V.A. Drozdov, S.A. Stuken, A.V. Bubnov, E.I. Grigorov, A.V. Kalinkin, V.I. Zaikovskii, Kinet. Catal. 32 (1991) 387–394.
[55] P.G. Tsyrulnikov, S.V. Tsybulya, G.N. Kryukova, A.I. Boronin, S.V. Koscheev, T.G. Starostina, A.V. Bubnov, E.N. Kudrya, J. Molec. Catal. 179 (2002) 213–220.
[56] G. Busca, Adv, Catal 57 (2014) 319–404.
[57] L. Liu, H. Yang, J. Wei, Y. Yang, Mater. Lett. 65 (2011) 694–697.
[58] F. Kapteijn, L. Smgoredjo, A. Andreini, J.A. Moulijn, Appl. Catal. B: Environ. 3 (1994), 173-169.
[59] F. Kapteijn, A.D. van Langeveld, J.A. Moulijn, A. Andreini, M.A. Vuurman, A.M. Turek, J.M. Jehng, I.E. Wachs, J. Catal. 150 (1994) 94–104.
[60] Aboukais, E. Abi-Aad, B. Taouk, Mater. Chem. Phys. 142 (2013) 564–571.
[61] H. Lieske, G. Lietz, H. Spindler, J. Volteri, J. Catal. 81 (1983) 8–16.
[62] C. Hwang, C. Yeh, J. Mol. Catal. A: Chem. 112 (1996) 295–302.
[63] M.J. Tiernan, O.B. Finlayson, Appl. Catal. B 19 (1998) 23–35.
[64] A.C.S.F. Santos, S. Damyanova, G.N.R. Teixeira, L.V. Mattos, F.B. Noronha, F.B. Passos, J.M.C. Bueno, Appl. Catal. A 290 (2005) 123–132.
[65] H. Lieske, J. Volter, J. Phys. Chem. 89 (1985) 1841–1843.
[66] R. Burch, F.J. Urbano, Appl. Catal. A: Gen 124 (1995) 121.
[67] R. Prins, Chem. Rev. 112 (2012) 2714–2738.
[68] T. Maillet, J. Barbier, D. Duprez, Appl. Catal. B: Environ. 9 (1996) 251–266.
[69] E. Garbowski, C. Feumi-Jantou, N. Mouaddib, M. Primet, Appl. Catal. A: Gen. 109 (1994) 277–291.
[70] R.G. Silver, J.C. Summers, W.B. Williamson, Stud. Surf. Sci. Catal. 71 (1991) 167–180.